

**BULLETIN N° 233**  
**ACADÉMIE EUROPEENNE**  
**INTERDISCIPLINAIRE**  
**DES SCIENCES**  
**INTERDISCIPLINARY EUROPEAN ACADEMY OF SCIENCES**



**Lundi 4 mars 2019 :**

**à 16h**

à l'Institut Henri Poincaré salle 01

11, rue Pierre et Marie Curie 75005 PARIS/Métro : RER Luxembourg

**Conférence :**

*"Modélisations multiéchelles pour la chimie mésoscopique: l'exemple de la chimie séparative"*

par Jean-François DUFREÛCHE, Professeur à l'Université de Montpellier  
 Laboratoire Modélisation Mésoscopique et Chimie Théorique (LMCT)

Institut de Chimie Séparative de Marcoule ICSM

UMR 5257 /CEA / CNRS / Université de Montpellier / ENSCM

**Notre Prochaine séance aura lieu le lundi 1er avril 2019 à 16h**

à l'Institut Henri Poincaré salle 421

11, rue Pierre et Marie Curie 75005 PARIS/Métro : RER Luxembourg

Elle aura pour thème

**Conférence:**

*" Progrès récents dans le transport de molécules au travers des membranes cellulaires, ou comment des molécules polaires de haut poids moléculaire peuvent traverser une barrière imperméable sans systèmes de transport spécialisés."*

par Sandrine SAGAN, Directrice de Recherche CNRS,

Laboratoire des Biomolécules (UMR 7203 CNRS-ENS-SU), Paris

# ACADÉMIE EUROPÉENNE INTERDISCIPLINAIRE DES SCIENCES INTERDISCIPLINARY EUROPEAN ACADEMY OF SCIENCES

**PRÉSIDENT** : Pr Victor MASTRANGELO  
**VICE PRÉSIDENT** : Pr Jean-Pierre FRANÇOISE  
**VICE PRÉSIDENT BELGIQUE**(Liège):  
 Pr Jean SCHMETS  
**VICE PRÉSIDENT ITALIE**(Rome):  
 Pr Ernesto DI MAURO  
**SECÉTAIRE GÉNÉRALE** : Irène HERPE-LITWIN  
**TRÉSORIÈRE GÉNÉRALE**: Édith PERRIER

**MEMBRE S CONSULTATIFS DU CA** :  
 Gilbert BELAUBRE  
 François BÉGON  
 Bruno BLONDEL  
 Michel GONDRAN

**PRÉSIDENT FONDATEUR** : Dr. Lucien LÉVY (†)  
**PRÉSIDENT D'HONNEUR** : Gilbert BELAUBRE

**CONSEILLERS SCIENTIFIQUES** :  
**SCIENCES DE LA MATIÈRE** : Pr. Gilles COHEN-TANNOUJJI  
**SCIENCES DE LA VIE ET BIOTECHNIQUES** : Pr Ernesto DI MAURO

**CONSEILLERS SPÉCIAUX**:  
**ÉDITION**: Pr Robert FRANCK  
**RELATIONS EUROPÉENNES** :Pr Jean SCHMETS  
**RELATIONS avec AX**: Gilbert BELAUBRE  
**RELATIONS VILLE DE PARIS et IDF**:  
 Michel GONDRAN et Claude MAURY  
**MOYENS MULTIMÉDIA et UNIVERSITÉS**: Pr Alain CORDIER  
**RECRUTEMENTS**: Pr. Sylvie DERENNE  
**SYNTHÈSES SCIENTIFIQUES**: Jean-Pierre TREUIL  
**MECENAT**: Pr Jean Félix DURASTANTI  
**GRANDS ORGANISMES DE RECHERCHE NATIONAUX ET INTERNATIONAUX**: Pr Michel SPIRO  
**THÈMES ET PROGRAMMES DE COLLOQUES**: Pr Jean SCHMETS

**SECTION DE NANCY** :  
**PRÉSIDENT** : Pr Pierre NABET

Mars 2019

**N°233**

TABLE DES MATIERES

p. 03 Séance du 4 mars 2019 :

p. 06 Documents

**Prochaine séance : lundi 1er avril 2019**

## **Conférence:**

*" Progrès récents dans le transport de molécules au travers des membranes cellulaires, ou comment des molécules polaires de haut poids moléculaire peuvent traverser une barrière imperméable sans systèmes de transport spécialisés."*

par **Sandrine SAGAN**, Directrice de Recherche CNRS,  
 Laboratoire des Biomolécules (UMR 7203 CNRS-ENS-SU), Paris

# **ACADEMIE EUROPEENNE INTERDISCIPLINAIRE DES SCIENCES**

**Fondation de la Maison des Sciences de l'Homme, Paris.**

**Séance du Lundi 4 mars 2019/IHP 16h**

La séance est ouverte à 16h sous la **Présidence de Victor MASTRANGELO** et en la présence de nos Collègues Gilbert BELAUBRE, Eric CHENIN, Françoise DUTHEIL, Claude ELBAZ, Irène HERPE-LITWIN, Claude MAURY, Marie-Françoise PASSINI, Jacques PRINTZ, Jean SCHMETS, Alain STAHL, Jean-Pierre TREUIL .

Etaient excusés :François BEGON, Jean-Pierre BESSIS, Bruno BLONDEL, Jean BERBINAU, Jean-Louis BOBIN, Michel CABANAC, Alain CARDON, Juan-Carlos CHACHQUES, Gilles COHEN-TANNOUDJI, Alain CORDIER , Daniel COURGEAU, Sylvie DERENNE, Ernesto DI MAURO, Jean-Felix DURASTANTI, Vincent FLEURY, Robert FRANCK, Jean -Pierre FRANCOISE, Michel GONDRAN, Jacques HENRI-ROBERT, Dominique LAMBERT, Pierre MARCHAIS, Anastassios METAXAS, Jacques NIO, Edith PERRIER, Pierre PESQUIES, Michel SPIRO, Mohand TAZEROUT, Jean-Paul TEYSSANDIER, Jean VERDETTI.

Etait présent notre collègue membre correspondant Benoît PRIEUR

## **I. Conférence du Pr Jean-François DUFRECHE**

### **A. Présentation du conférencier par notre Président Victor MASTRANGELO.**

#### **Jean-François DUFRECHE**

Professeur à l' Université de Montpellier,  
Institut de Chimie Séparative de Marcoule, UMR CNRS/CEA/Université Montpellier 2/ENSCM  
Directeur du Laboratoire de Modélisation Mésoscopique et de Chimie Théorique (LMCT/ICSM)  
Adresse site : [www.icsm.fr](http://www.icsm.fr)

#### **Formation et carrière universitaire :**

Depuis 2009: professeur Université Montpellier and à l'Institut de Chimie Séparative de Marcoule (ICSM)  
2003-2009: Chargé de Recherche CNRS laboratoire PECSA (Université Paris 6-UPMC)  
2001-2003: Post-Doc University of Cambridge (UK) Department of Chemistry  
1999-2001: Doctorat Université Paris 6-UPMC Laboratoire liquides ioniques et interfaces chargées  
1998-1999: CEA/DAM Département de Physique théorique et appliquée  
1994-1999: Ecole Normale Supérieure de Lyon

#### **Centres d'Intérêt de recherche (mots clés)**

Chimie de séparation, Descriptions multi-échelles, Solutions d'électrolytes , Suspensions chargées, Milieux confinés. Propriétés structurales et dynamiques des systèmes de matière molle. Gros grains.  
Thermodynamique statistique . Chimie théorique. Dynamique moléculaire. Simulations de Monte Carlo.

#### **Activités d'Enseignement**

- Supervision de 12 doctorants (3 ongoing)
- Environ 200 heures par an d'enseignement de Chimie physique à tous les niveaux universitaires depuis 2009

### Evaluation, Récompenses & Financements:-

- h-factor = 23, nombre total de citations = 1334, 209 citations en 2018
- 
- Direction du groupe du laboratoire de Modélisation et de Chimie théorique (9 chercheurs: 3 permanents, 3 Docteurs and 3 post docs).
- Évaluation positive AERES du groupe : A+ and A in 2010 and 2015
- Prix du magazine “La Recherche” (section Energie, co-lauréat, 10 000 €)
- Projet senior ERC, REE-CYCLE (sup. Th. Zemb) 2013
- 6 ANR (2009, 2008 2013 2015 2016 2018)
- Invitation à 19 conférences internationales – 17 invitations à des conférences nationales
- Professeur invité : Monastir (Tunisie) 2015
- Organisation de 4 ateliers et deux conférences internationales
- Membre de la section CNU 31 2011-2015
- Éditeur associé de Pure and Applied Chemistry (2012)

### Publications

90 articles ( dans des revues internationales à comité de lecture)

19 invitations dans des conférences internationales, 58 communications orales dans des conférences internationales

### Cinq publications représentatives:

[1] Multicomponent Model for the Prediction of Nuclear Waste/Rare-Earth Extraction Processes M. Špadina, K. Bohinc, Th. Zemb, J.-F. Dufrêche, *Langmuir*, **34**, 10434 (2018)

[2] Selective layer-free blood serum ionogram based on ion-specific interactions with a nanotransistor Transistors R. Sivakumarasamy, R. Hartkamp, B. Siboulet, J.-F. Dufrêche, K. Nishiguchi, A. Fujiwara, N. Clément *Nature Materials* **17**, 464 (2018)

[3] How Ion Condensation Occurs at a Charged Surface: A Molecular Dynamics Investigation of the Stern Layer for Water–Silica Interfaces S. Hocine, R. Hartkamp, B. Siboulet, M. Duvail, B. Coasne, P. Turq, J.-F. Dufrêche, *J. Phys. Chem. C*, **120**, 963 (2016)

[4] Hydrophobic Transition in Porous Amorphous-mediated interactions between charged and neutral nanoparticles. B. Siboulet, B. Coasne, J. F. Dufrêche and P. Turq, *J. Phys. Chem. B*, **115**, 7881 (2011)

[5] Ion transport in porous media: derivation of the macroscopic equations using upscaling and properties of the effective coefficients" <sup>[SEP]</sup>G. Allaire, R. Brizzi, J.-F. Dufrêche, A. Mikelic and A. Piatnitski, <sup>[SEP]</sup>*Computat. Geosci.*, **17**(3), 479 (2013)

## B. Conférence

### Résumé de la conférence du Pr DUFRÊCHE:

#### Modélisations multiéchelles pour la chimie mésoscopique: l'exemple de la chimie séparation

La chimie séparative présentée dans cette conférence consiste à séparer les différents éléments chimiques pour obtenir des matériaux purs ou destinés au recyclage. Elle met en œuvre des techniques comme l'extraction liquide-liquide ou la flottation qui utilisent des états de la matière complexes

(microémulsions, états colloïdaux, mousses). Ceux-ci sont structurés à l'échelle intermédiaire (mésoscopique) et cette complexité particulière jouent un rôle fondamental pour le processus de séparation.

Nous montrerons comment les méthodes modernes de modélisation peuvent traiter ces systèmes de façon cohérente, à la fois pour les propriétés d'équilibre et pour celles de transport. D'un point de vue moléculaire, par une suite de moyennes et approximations on peut décrire ces fluides complexes de façon cohérente aux différentes échelles impliquées. Le rôle des outils numériques et des principes physiques sera particulièrement souligné. Nous montrerons comment ces nouveaux systèmes révolutionnent les approches macroscopiques thermodynamiques utilisées jusqu'à présent.

Un compte-rendu détaillé, voire **un enregistrement audio-vidéo** agréé par le conférencier, sera prochainement disponible sur le site de l'AEIS <http://www.science-inter.com>.

### **REMERCIEMENTS**

Nous tenons à remercier vivement Mme Sylvie BENZONI Directrice de l'Institut Henri POINCARÉ et Mmes Florence LAJOINIE et Chantal AMOROSO ainsi que les personnels de l'IHP pour la qualité de leur accueil.

## Documents

– Pour préparer la conférence de **Sandrine SAGAN** , nous vous proposons :

p. 07 : un résumé de sa conférence

p. 08 : un article intitulé "*Membrane Crossing and Membranotropic Activity of Cell-Penetrating Peptides: Dangerous Liaisons?*" par Walrant A, Cardon S, Burlina F, **Sagan S**, paru dans *Acc Chem Res.* 2017 Dec 19;50(12):2968-2975.

– Pour compléter la conférence du Pr **Jean-François DUFRECHE** nous vous proposons:

p. 21 : un article intitulé "*Multicomponent Model for the Prediction of Nuclear Waste/Rare-Earth Extraction Processes*" par M. Špadina, K. Bohinc, Th. Zemb, **J.-F. Dufreche**, publié dans *Langmuir*, 34, 10434 (2018)

Résumé :

***Progrès récents dans le transport de molécules au travers des membranes cellulaires, ou comment des molécules polaires de haut poids moléculaire peuvent traverser une barrière imperméable sans systèmes de transport spécialisés.***

Sandrine Sagan, Directrice de Recherche CNRS, Laboratoire des Biomolécules (UMR 7203 CNRS-ENS-SU), Paris.

Les membranes sont présentes à tous les niveaux d'organisation des organismes vivants. Longtemps présentée comme une barrière passive séparant la cellule de son environnement, la membrane plasmique joue un rôle majeur dans l'homéostasie cellulaire en assurant des fonctions dynamiques cruciales de contrôle et de traitement de l'information en réponse aux nombreux stimuli extérieurs. Malgré sa composition moléculaire simple (lipides, protéines, glucides), son organisation spatio-temporelle complexe confère à la membrane plasmique des propriétés de déformation, courbure et d'élasticité très dynamiques. Des systèmes protéiques de transport actif sophistiqués contrôlent les échanges à travers la membrane pour importer des nutriments essentiels. Depuis une trentaine d'années, il est connu que des nanoobjets de taille importante et polaires comme des peptides ou des protéines sont capables de traverser la membrane plasmique sans utiliser ses systèmes de transport actifs. J'illustrerai à l'aide d'exemples récents les aspects physico-chimiques qui permettent d'appréhender et dévoiler ces nouveaux mécanismes de passage des membranes.

See discussions, stats, and author profiles for this publication at: <https://www.researchgate.net/publication/321324538>

# Membrane Crossing and Membranotropic Activity of Cell-Penetrating Peptides: Dangerous Liaisons ?

Article in *Accounts of Chemical Research* · November 2017

DOI: 10.1021/acs.accounts.7b00455

CITATIONS

6

READS

135

4 authors:



**Astrid Walrant**

Pierre and Marie Curie University - Paris 6

22 PUBLICATIONS 352 CITATIONS

[SEE PROFILE](#)



**Sébastien Cardon**

University of Leeds

4 PUBLICATIONS 6 CITATIONS

[SEE PROFILE](#)



**Fabienne Burlina**

Pierre and Marie Curie University - Paris 6

106 PUBLICATIONS 1,401 CITATIONS

[SEE PROFILE](#)



**Sandrine Sagan**

French National Centre for Scientific Research

158 PUBLICATIONS 3,198 CITATIONS

[SEE PROFILE](#)

Some of the authors of this publication are also working on these related projects:



backbone protection [View project](#)

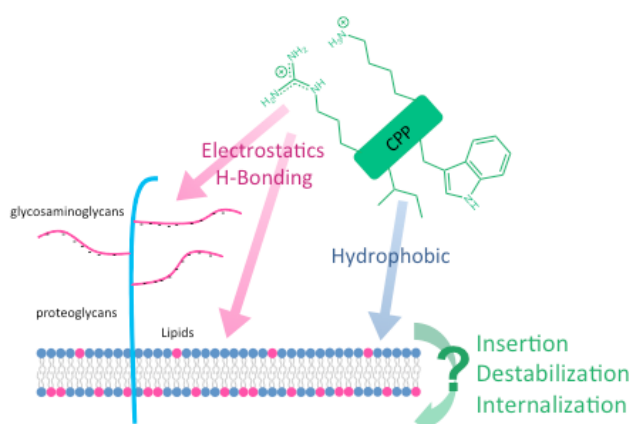
## Membrane crossing and membranotropic activity of cell-penetrating peptides: *Dangerous liaisons?*

Astrid Walrant<sup>1</sup>, Sébastien Cardon<sup>1</sup>, Fabienne Burlina<sup>1</sup> and Sandrine Sagan<sup>1\*</sup>

<sup>1</sup>Sorbonne Universités, UPMC Univ. Paris 06, École normale supérieure, PSL Research University, CNRS, Laboratoire des Biomolécules (LBM), 4 place Jussieu, 75005 Paris, France

\*Corresponding author : sandrine.sagan@upmc.fr

### Conspectus



Living organisms have to maintain a stable balance in molecules and ions in the changing environment in which they are living, a process known as homeostasis. At the level of cells, the plasma membrane has a major role in homeostasis, since this hydrophobic film prevents passive diffusion of large/hydrophilic molecules between the extracellular and intracellular milieu. Living organisms have evolved with highly sophisticated transport systems to control exchanges across this barrier: import of nutrients and fuel essential for their survival; recognition of chemical or physical messengers allowing information interchanges with surrounding cells. Beside specialized proteins, endocytosis mechanisms at the level of the lipid bilayer can transport molecules from the outside across the cell membrane, in an energy-dependent manner.

The cell membrane is highly heterogeneous in its molecular composition (tens of different lipids, proteins, polysaccharides and combinations of these) and dynamic with bending, deformation and elastic properties that depend on the local composition of membrane domains. Many viruses, microorganisms and toxins exploit the plasma membrane to enter into cells. Chemists develop strategies to target the plasma membrane with molecules capable of circumventing this hydrophobic barrier, in particular to transport and deliver nonpermeable drugs in cells for biotechnological or pharmaceutical perspectives. Drug delivery systems are numerous and include lipid-, sugar-, protein- and peptide-based delivery systems, since these biomolecules generally have good biocompatibility, biodegradability, environmental sustainability, cost effectiveness and availability. Among those, cell-penetrating peptides (CPPs), reported for the first time in the early 1990's, are attracting major interest not only as potential drug delivery systems, but also at the level of fundamental research. It was indeed demonstrated very early that these peptides, which generally correspond to highly cationic sequences, can still cross the cell membrane at 4°C, a temperature at which all active transport and endocytosis pathways are totally inhibited. Therefore, how these charged hydrophilic peptides cross the hydrophobic membrane barrier is of utmost interest as a pure basic and physico-chemical question.

In this Account, we focus on cationic cell-penetrating peptides (CPPs), and the way they cross cell membranes. We summarize the history of this field that emerged around 20 years ago. CPPs were indeed first identified as protein-transduction domains from the human immunodeficiency virus (HIV) TAT

protein and the Antennapedia homeoprotein, a transcription factor from *Drosophila*. We highlight our contribution to the elucidation of CPP internalization pathways, in particular translocation, which implies perturbation/reorganisation of the lipid bilayer, and endocytosis depending on sulfated glycosaminoglycans. We show a particular role of Trp (indole side chain) and Arg (guanidinium side chain), which are essential amino acids for CPP internalization. Interactions with the cell-surface are not only Coulombic; H-bonds and hydrophobic interactions contribute also significantly to CPP entry. The capacity of CPPs to cross cell membrane is not related to their strength of membrane binding. Finally, we present optimized methods based on mass spectrometry and fluorescence spectroscopy, that allow unequivocal quantification of CPPs inside cells or bound to the outer leaflet of the membrane, and discuss some limitations of the technique of flow cytometry that we have recently highlighted.

## Introduction

A plethora of proteins have been reported for their capacity to cross cell membranes. Cell-penetrating proteins are found ubiquitously within living organisms, from viruses and bacteria, to plant and animal cells. They have very different biological functions, being detrimental when working in the context of bacterial or viral invasion of animal cells, or being crucial for the life of metazoans, as exemplified by the case of the homeoprotein transcription factors during development and adulthood of animals. Homeoproteins are of particular interest because they possess unique and unconventional cell transfer paracrine properties, being secreted by some cells and internalized into others. To understand how these proteins act to penetrate cells at the level of the plasma membrane, structure-activity relationship (SAR) studies can be done. Protein engineering and peptide synthesis indeed allow exploring protein domains that are responsible for the membrane crossing properties of these proteins.

In the early 1990s, such SAR studies led to the identification of the first protein-transduction domains (PTDs) capable to cross cell membranes: the Tat peptide (GRKKRRQRRRPQ) derived (region 48-59) from the transactivator of transcription (TAT) of the human immunodeficiency virus (HIV)<sup>1,2</sup>, and the Penetratin peptide (RQIKIWFQNRRMKWKK) derived (region 341-356) from the *Drosophila* homeoprotein *Antennapedia*<sup>3,4</sup>. These PTDs led to the emergence of the field of cell-penetrating peptides (CPPs), which attract much interest for therapeutical or pharmaceutical applications. CPPs were indeed early evidenced as efficient delivery systems for high molecular weight and hydrophilic molecules (oligonucleotides, proteins, antibodies etc) conjugated to their sequence<sup>5</sup>. However, beside unfavorable pharmacokinetics (mainly resulting from their rapid renal clearance), the therapeutical use of CPPs is still hampered, principally because these peptides have no cell specific entry. Some strategies have been reported to overcome this lack of specificity, but require in general hard chemistry work, a major drawback to further consider these molecules for technological or therapeutical applications. Alternatively, the emergence of cell-penetrating homing peptides is particularly promising for targeting specific cells and tissues in the context of pathologies such as cancers. These peptides indeed bind tumor-specific receptors and enhance internalization of conjugated or unconjugated payload drugs (antibodies, nanoparticles etc) through a specific bulk endocytosis (macropinocytosis-like) pathway<sup>6</sup>.

Understanding the molecular mechanisms and internalization pathways of these peptides, represents an alternative and complementary approach for the rational design of efficient CPPs with improved cell specific delivery. This review is focused on our current view of the molecular mechanisms and internalization pathways of CPPs, with a particular emphasis on their detection and quantification inside cells in relation with their membranotropic activities.

The first reported CPP sequences, Tat and Penetratin, are highly cationic peptides with an average charge of +0.67 and +0.44 per amino acid, respectively. This common feature led to the general idea that cell-penetrating peptides are only cationic sequences. However, tens of new CPPs have now been described, among which some are negatively charged and/or amphipathic<sup>5</sup>. In principle, the two peptide sequences, Tat and Penetratin, should be synthesized with blocked *N*- and *C*-terminal ends, to mimic the peptide sequence as it is in the original protein. In addition to the cationic residues, the Tat peptide contains 2 polar (2 Q) and 2 nonpolar (G, P) uncharged amino acids. The Tat peptide is a pure basic sequence unstructured in solution or in interaction with phospholipids or GAGs<sup>7,8</sup>. In the context of the full TAT protein, this sequence also shows high conformational variability in its secondary structure<sup>9</sup>. On its side, the Penetratin sequence includes 3 polar (2 Q, N) and 6 nonpolar (2 I, 2 W, M, F) uncharged amino acids. This peptide is a secondary amphipathic peptide when structured as a  $\alpha$ -helix. Penetratin free in solution has no particular secondary structure and adopts a chameleon-like structure in complex, being

either a  $\alpha$ -helix or  $\beta$ -strand, depending on the stoichiometry and the interacting partner<sup>10,7,8</sup>. In the context of the homeoprotein, the Penetratin peptide corresponds to the highly stable third helix (without the first E residue) of the homeodomain<sup>4</sup>.

The amino acid composition confers to each peptide specific physico-chemical properties, which are crucial to control their interaction with cell-surface molecules and to trigger efficient entry into cells. With regard to the cell-surface, peptides first meet the glycocalyx, a thick and viscous layer of membrane-inserted proteoglycans and floating polysaccharidic moieties, located on the external side of the plasma membrane. Glycosaminoglycans (GAGs) are the polysaccharide part of the proteoglycans. They are linear anionic polymers with different size and content of sulfated disaccharides, which constitute in particular chondroitin (CS) and heparan (HS) sulfates<sup>11</sup>. GAGs are highly dynamic at the cell-surface, half of these membrane-bound molecules are secreted in the cell medium, and the other half is subject to endocytotic internalization and degradation. Both processes have kinetics in the range of hours<sup>12</sup>. Below the glycocalyx, the lipid bilayer is constituted in animal cells mostly of zwitterionic phosphatidylcholine phospholipids with one cis-unsaturated fatty acyl chain, which renders them fluid at physiological temperature<sup>13</sup>. Some membrane domains are enriched in sphingomyelin and cholesterol and act as functional platforms, in which are found for instance ligand-induced clusters of syndecans<sup>14</sup>, some proteoglycans containing both anionic HS and CS<sup>15</sup>. In addition, some domains include phospholipids such as phosphatidylethanolamine (PE) that have the propensity to induce negative curvature in the membrane<sup>16</sup>. Membrane lipids are also synthesized and renewed in the time scale of few hours<sup>17</sup>.

The plasma membrane of animal cells, with its well-defined lateral and transversal supramolecular organization in relation with the molecular composition of specific domains in glycoproteins, polysaccharides and lipids, is therefore a highly complex and heterogeneous structure. In addition, the cellular environment might vary. Local changes in the membrane potential and pH modulate the physico-chemistry of the membrane, which impacts on its bending and fluidity properties. Altogether, when the question of membrane crossing of peptides and proteins is addressed, one should consider globally their chemical reactivity and physico-chemistry properties in relation with the membrane environment. For instance we identified very effective thiol-specific pathways of internalization for CPPs containing cysteine or cystine in their sequence<sup>18,19</sup>.

### **Internalization pathways of CPPs: where do we stand?**

A general property of cell-penetrating peptides is their capacity to interact with plasma membranes. It was originally demonstrated that oligolysine were less efficiently internalized than oligoarginine peptides<sup>20, 21, 22</sup>. This finding highlighted the importance of bidentate hydrogen bonds between guanidinium groups and natural (phosphate moieties of phospholipids) or synthetic (pyrenebutyrate added to cells together with oligoarginines) counterions for crossing directly the membrane<sup>23, 24</sup>, a process known as translocation. Translocation implies that the peptide enters directly into the cytosol of the cell (Figure 1). Bidentate hydrogen bonds of arginine with hydrophobic counterions indeed result in the partition of the ion-pair complex into the lipid bilayer and its diffusion across, likely according to the membrane potential. Other molecular mechanisms have been proposed to explain direct membrane crossing, such as the formation of transient pores<sup>25</sup> or of inverted micelles<sup>26</sup>.

Translocation still occurs at low temperature (<12°C), although with reduced efficiency because the membrane fluidity, the lipid membrane asymmetry and the membrane potential are energy-dependent processes. Besides, endocytosis pathways are major mechanisms reported for CPP internalization, principally through macropinocytosis<sup>27</sup>. These pathways are fully energy and temperature dependent, being inhibited at temperature below 12°C<sup>28</sup>, while the use of endocytosis inhibitors presents major drawbacks regarding cell selectivity and cytotoxicity<sup>29</sup>. Therefore, to study the respective contribution of endocytosis and translocation, we favor the use of different temperatures.

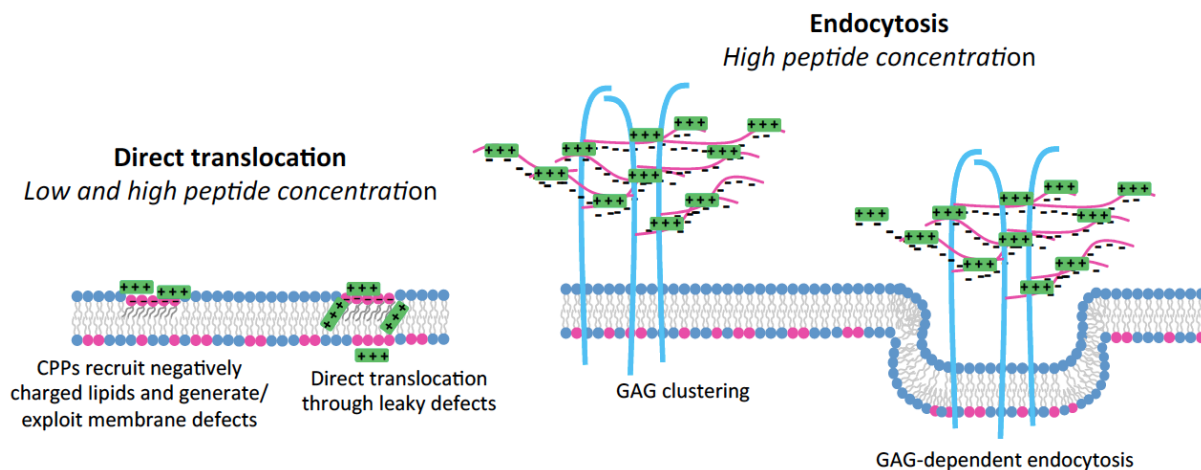


**Figure 1** - Internalization of CPPs involves two major general pathways: translocation and GAG-dependent endocytosis. At low micromolar concentration, CPPs recruit negatively charged lipids and/or exploit membrane defects to translocate into cells<sup>50</sup>; They also bind sulfated GAGs of cell-surface proteoglycans. At higher micromolar concentrations, CPPs still translocate into cells, and also induce clustering of proteoglycans and endocytosis.

By quantifying the absolute amount of internalized peptide for a series of CPPs (Tat, Penetratin, R9, RW9 ...), we confirmed the crucial role of anionic GAGs in the mechanism of internalization<sup>30</sup> (Figure 1). This result was obtained by comparing the internalization efficacy of CPPs in wild-type cells and a cell line genetically deficient in HS and CS expression<sup>11</sup>. Most CPPs we have studied had dramatic decreased internalization at 4°C compared to 37°C in WT cells<sup>30</sup>. This was not the case for GAG-deficient cells in which the CPPs had very similar internalization efficacy at both temperatures, close to the one observed in WT cells at 4°C (Figure 2). These results show that the endocytosis pathway of these CPPs mostly relies on the presence of GAGs at the cell-surface. Interestingly, this is not the case for Tat peptide which internalizes in similar quantities in WT and GAG-deficient cells at 37°C and 4°C<sup>30</sup>. Importantly, further analysis showed that at low micromolar CPP concentration (<2-3 μM) and 37°C, or any concentration up to 10 μM at 4°C, the presence/absence of cell-surface GAGs or sialic acids makes no longer differences in the internalization efficacy of different CPPs<sup>30-32</sup> (Figure 2). These results indicate that at 37°C for low micromolar concentrations of peptides, only translocation occurs, while GAG-dependent internalization is a cooperative process and requires accumulation of the peptides at the cell-surface. In addition, at 4°C, translocation is the only effective internalization pathway and is not dependent on the cell-surface composition.

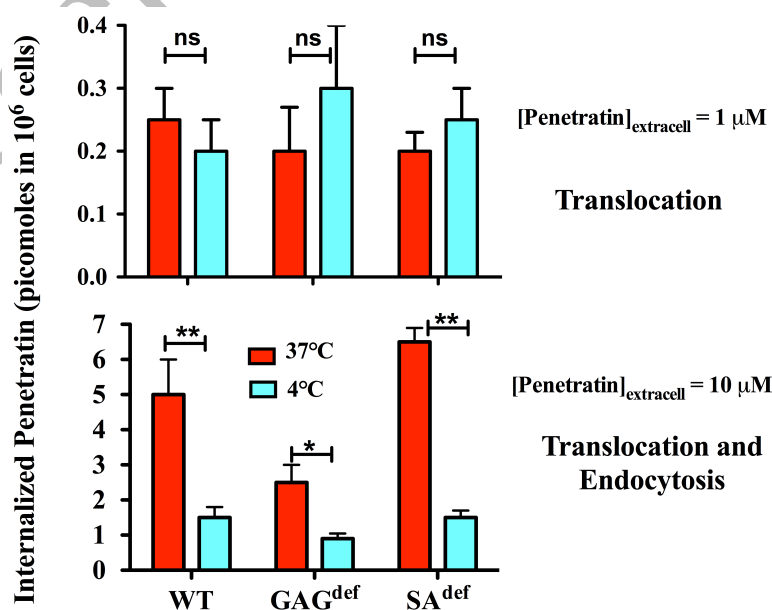


**Figure 2:** Translocation is observed at 1  $\mu\text{M}$  [Penetratin] at 37°C (red) and 4°C (blue), while at higher concentration (illustrated herein for 10  $\mu\text{M}$ ) both endocytosis (37°C) and translocation (37°C and 4°C) are active internalization pathways. At 37°C, since Penetratin is less internalized in GAG-deficient cells, its internalization relies on the presence of cell-surface proteoglycans (HS and CS), while the peptide internalized more in cells lacking sialic acids at the cell-surface (SA<sup>def</sup>). ns, not significant; \* significant; \*\* very significant.

GAGs are thus essential partners for internalization of many CPPs<sup>33</sup>. Sulfated proteoglycans are located in dynamic transient microdomains enriched in cholesterol and sphingomyelin (SM), and cluster into larger platforms in response to specific stimuli such as ligand binding to membrane receptors. We showed that sphingomyelin hydrolysis (in ceramide) or cholesterol depletion in the cell membrane, affects both translocation and endocytosis<sup>34</sup>, results we explain as follows: i) CPPs can bind and cluster GAGs that act as autonomous receptors and, then follow a specific endocytosis pathway. Alternatively, in the domains from which GAGs are absent, CPPs can recruit and cluster specific membrane lipids, to evoke or stabilize locally, and exploit membrane thinning and defects to translocate. Penetratin for instance shows strong preference for unsaturated phospholipids found in disordered domains as we demonstrated using a photolabeling strategy<sup>35</sup>. The kinetics of a given CPP to partition between cell surface GAGs and in defect regions of the lipid bilayer would determine the balance between endocytosis and translocation pathways of internalization. Of interest is that we could identify that the effects of sphingomyelinase treatment or cholesterol depletion was massive on the entry of Trp-containing CPPs in WT cells, contrasting with the situation in GAG-deficient cells<sup>34</sup>. These results converge with another study in which we demonstrated for the first time that Trp residues in CPPs enhance dramatically the enthalpy of binding of the peptides with HS and CS, and the clustering of GAGs, thus establishing a role of Trp not only interfacial at the level of the lipid bilayer but also crucial at the level of the glycocalyx, involving potential ion-pair  $\pi$  interactions<sup>32, 36</sup>. Altogether, delineating a general internalization pathway for all CPPs is rather difficult, because CPP sequences differ from one another and can interact with a plethora of molecules at the cell-surface. The current view is that there are two major pathways of internalization: direct translocation across the plasma membrane (transient pore formation, carpet model, inverted micelles etc), and endocytosis that includes bulk (macropinocytosis) and receptor-dependent (clathrin- or caveolin-mediated) processes<sup>5, 28, 33, 36</sup>.

### **Lack of relationship between membranotropic activity and internalization efficacy of CPPs**

To enter into cells, cationic peptides first interact with membrane components. However, binding of a peptide to the cell membrane is not directly related to its capacity of crossing it. For instance, we have studied two related cationic and secondary amphipathic sequences, RW9 (RRWRRRWR) and RL9 (RLLRRLRR). These two peptides have the same number of positive charges, and contain 3 nonpolar residues at the same position in the sequence, either W or L. The peptide RW9<sup>37</sup> is internalized twenty-fold better than RL9 in cells<sup>38</sup>. But, both peptides bind to the cell membrane, with only a two-fold difference in the quantity of membrane-bound species, that remain after washings, respectively 100 and 250 pmoles for RL9 and RW9. A full analysis of the interaction of the peptides with model membranes underlined a deeper insertion of RL9 compared to RW9 into the lipid bilayer, despite an apparent dissociation constant value of respectively 7.5 and 1.5  $\mu\text{M}$  for POPG LUVs<sup>39</sup>. The two peptides have similar affinity for heparin with K<sub>d</sub> values of 80 nM (RL9) and 10 nM (RW9)<sup>32</sup>. The fact that a peptide that does not cross the membrane, inserts deeper, is at first glance a counter intuitive result. We further showed that RL9 is retained close to the membrane core region and that this peptide tends to increase lipid ordering around itself. This observation supports the lack of membrane crossing of the peptide, since membrane reorganization leading to RL9 crossing the membrane would indeed be energetically extremely unfavorable. Altogether, these results show that membrane binding should not be used to predict the capacity of a peptide to cross cell membranes (Figure 3).

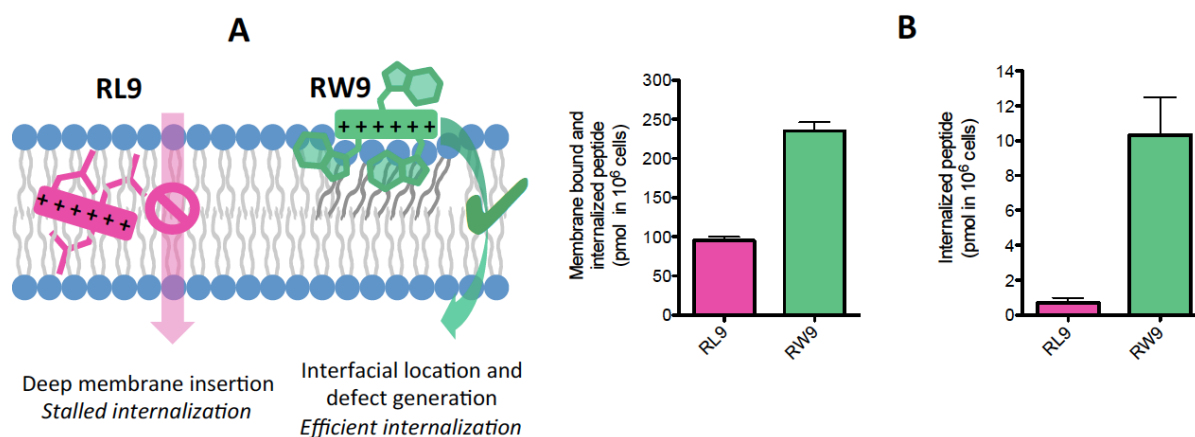


**Figure 3-** The absence of relationship between membrane binding and cell-penetration activity is illustrated with two amphipathic peptides. **A)** RL9 binds to the lipid bilayer, inserts deeply within the acyl chains and fails to cross the membrane; RW9 binds to the lipid bilayer at the water/lipid interface and has efficient membrane translocation function<sup>39</sup>. **B)** MS quantification of cell-associated (membrane-bound and internalized) or internalized peptides<sup>39</sup>.

Other experimental evidences reinforce this assumption. As mentioned above, it is possible to quantify the peptides that remain associated to cells after washings, which includes the membrane-bound and the internalized species<sup>40</sup>. We have shown that the membrane-bound peptide fraction, which is not washable, generally represents from 5- up to more than 100-folds the internalized peptide fraction. As long as the peptides are sensitive to enzymatic cleavage, it is possible to remove this membrane-bound species for example by trypsin (37°C) or pronase (4°C) treatment of cells, leaving for quantification only the internalized fraction of peptide<sup>40, 30</sup>. Using this method, we could stress for different CPP sequences (Tat, R9, RW9, Penetratin etc) that their accumulation and binding at the cell-surface do not reflect their internalization efficacy<sup>40, 30</sup>. For instance, after 1 h incubation followed by washings, Penetratin remains associated to similar extent to wild-type (240 pmoles), (HS and CS) GAG-deficient (220 pmoles) and sialic acid- (SA) deficient (360 pmoles) cells, albeit its internalization efficacy strongly differs (respectively 5, 2.5 and 6.5 pmoles) in the three cell lines<sup>30, 31</sup>. These results obtained with these cell lines having different membrane composition, further suggest that the non-washable fraction of peptides is retained at the level of the lipid bilayer. This observation is similar at 37°C and 4°C, although for some CPPs the quantity of membrane-bound species can be higher at 4°C, likely because the membrane is less fluid and has decreased conformational freedom and dynamics: some membrane-bound peptides would then be even less washable than at 37°C.

### Thermodynamics and kinetics of peptide binding to cell membrane

The fact that the non-washable membrane-bound fraction of peptides is found at the level of the lipid bilayer questions the thermodynamics and kinetics of the system. Indeed, it has long been reported unequivocally by different groups, including ours, that CPPs have more favorable binding thermodynamics, about one order of magnitude, for highly sulfated polysaccharides compared to any type of phospholipid, even negatively charged<sup>41, 31, 32</sup>. The binding affinity is indeed generally in the nM range for negatively charged polysaccharides and in the  $\mu$ M range for phospholipids (Figure 4).

We used cell-derived membranes to confirm the latter observation obtained with model membranes<sup>31</sup>. Penetratin has a dissociation constant of 10 nM for WT cell membrane. Its affinity is decreased for GAG-deficient cell membrane with a Kd value of 2  $\mu$ M. Interestingly, the Kd value is 200 nM for SA-deficient cells, in which (10  $\mu$ M) Penetratin internalizes better compared to WT cells. Moreover, the dissociation constant for WT cell membrane is very close to the one for heparin and CS, while the Kd for GAG-deficient cell membrane is closer to the one for phospholipids<sup>42</sup>. In addition, the thermodynamics of Penetratin interaction with model membranes of Egg PC/DOPE (1:1) is similar to the one of Egg PC/POPG (1:1)<sup>31</sup>. Therefore, binding of Penetratin to the lipid bilayer does not only rely on Coulombic interactions, the shape of the lipid headgroup and/or the membrane curvature in PE-enriched membrane domains also have a major contribution. We could confirm this assumption using photolabeling of PC phospholipids with which Penetratin interacts at the level of the lipid/water interface<sup>35</sup>.

In terms of kinetics, Penetratin binds similarly to the membrane of the three cell types<sup>30</sup>, with a  $k_{on}$  value of  $10^4 \text{ M}^{-1}\text{s}^{-1}$ <sup>31, 42</sup>, showing that the presence of anionic GAGs does not prevent the cationic peptide from interacting at the level of the lipid bilayer, despite the differences in the affinity of the peptide for the three cell membranes ( $K_d = k_{off}/k_{on}$ ), respectively 0.01, 0.2 and  $2 \mu\text{M}$  for WT, SA-deficient and GAG-deficient cells. This result implies that dissociation kinetic constants are much faster for membranes lacking GAGs than for membranes containing GAGs at their surface. Penetratin indeed dissociates 200-fold faster from the surface of GAG-deficient cells than from the surface of WT cells<sup>31, 42</sup>. Furthermore, these dissociation kinetic constants are similar between GAG-deficient cells and lipid model membranes, suggesting that the high dynamics of peptide/lipid complexes is a key step for translocation across the lipid bilayer. Altogether, these results again demonstrate that membrane binding and thermodynamics alone do not reflect the internalization capacity of CPPs. Thermodynamics would favor GAG-dependent internalization pathway, while kinetics reveal the dynamical interaction between CPPs and lipids and favor translocation. Internalization of a CPP is thus a subtle balance between these two pathways.

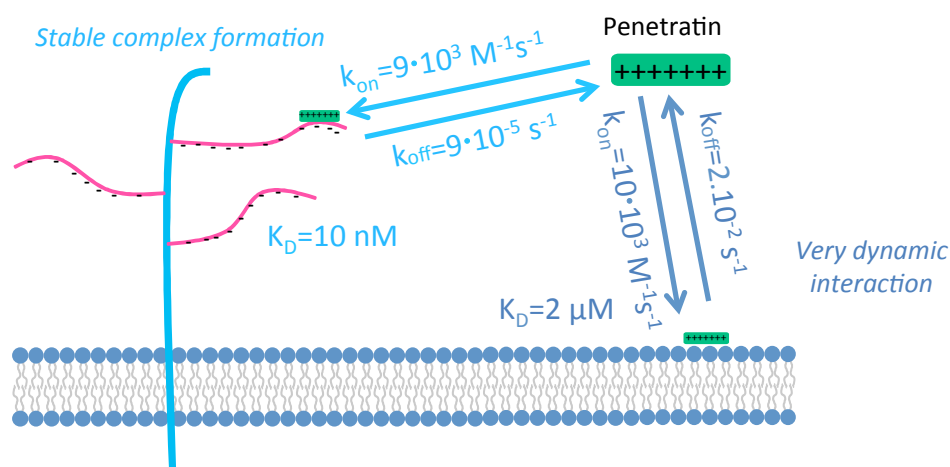


**Figure 4** - Thermodynamics favor interaction of Penetratin with anionic GAGs, while kinetics favor its interaction with the lipid bilayer. Data obtained by plasmon waveguide resonance spectroscopy<sup>31</sup>.

Translocation is the first internalization pathway in motion (at low extracellular CPP concentrations). With increasing concentrations of peptide, its accumulation on GAGs at the cell-surface leads to clusters of proteoglycans and endocytosis<sup>14, 43</sup>. Because the quantity of membrane-bound peptide always dominates the internalized one, caution should be taken when studying CPP entry, to ensure the complete elimination or the accurate determination of the membrane-bound or -trapped fraction of the peptide. We have contributed to this latter experimental aspect, developing reliable and robust methods to quantify membrane-bound and/or peptides internalized in cells.

#### Methods to study membrane-trapped or internalized CPPs: optimization and pitfalls

With the advent of the field of cell-penetrating peptides, came indeed the question of detection of peptides inside cells. More than ten years ago, we developed a method based on MALDI-TOF mass spectrometry (MS) to measure absolute quantities of peptides inside cells. Since this protocol has been reviewed several times<sup>44, 19, 45</sup>, we just give a brief overview herein. Two identical peptide sequences are synthesized with a biotin-bait in a spacer arm, which is or not isotopically labeled at the *N*-terminal of the sequence. Biotin slightly increases the hydrophobicity of the peptide but allows selective extraction of the peptides after cell lysis and the isotope labeled (deuterium) peptide is used as an internal standard for MS quantification. Briefly, after incubation of a controlled number of cells (generally one million) with the CPP, cells are washed. The membrane-bound peptide is kept intact when cells are only extensively washed with culture medium, and can be removed by enzymatic degradation (trypsin at  $37^\circ\text{C}$  and pronase at  $4^\circ\text{C}$ ). Cells are lysed with a high salt detergent solution containing a relevant amount of the isotope labeled version of the same CPP. The two peptides are then captured from lysed cells on streptavidin-coated magnetic beads. After drastic washings (high salt, SDS etc) of the beads, elution of the peptides is obtained at acid pH with the MALDI matrix  $\alpha$ -cyano-4-hydroxycinnamic acid. The absolute amount of the internalized CPP is calculated from the ratio of the unlabeled and labeled isotope mass of the CPP in the mass spectra. This robust method has proven very helpful to quantify membrane-bound internalized

peptide amounts, to study the mechanisms of internalization of CPPs, as well as their transport efficacy by quantifying directly a conjugated cargo peptide<sup>46, 47, 18, 37</sup>. In addition this method allows the analysis of the intracellular degradation of the CPPs or peptide cargoes. Interestingly, we have found CPPs such as Tat, Penetratin, R9 and RW9 to be stable inside cells within a few hours incubation, since, the most abundantly detected species corresponds to the intact peptide<sup>19, 37, 40</sup>. A modified analogue of RW9 allowed us to determine that the intact peptide represents 60% of the ion species detected after 1h15 incubation and 30% after 18 hours<sup>37</sup>.

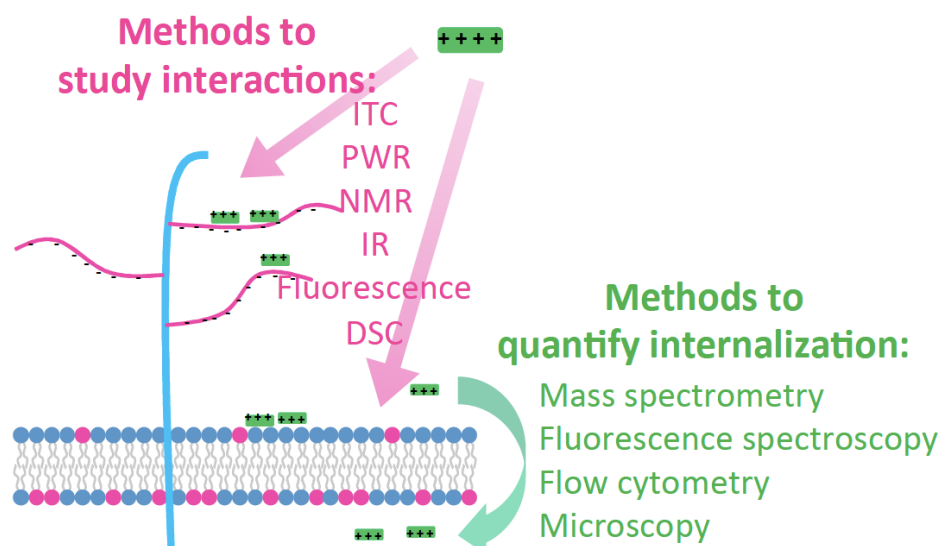


**Figure 5** - Current methods used to study peptide interaction with membranes or internalization in cells. ITC, isothermal calorimetry; DSC, differential scanning calorimetry; NMR, nuclear magnetic resonance spectroscopy; IR, infrared spectroscopy.

Fluorescence currently remains the most used method to detect peptides in cells, either by fluorescence imaging or flow cytometry. We evaluated the robustness and reliability of cytometry for the quantification of CPPs in cells and proposed an optimized method based on fluorometry allowing absolute quantification. As a premise, we have to note that the presence of a fluorescent label can in some cases shift the cytotoxicity of CPPs to lower concentrations. This is not surprising since these dyes are generally large and hydrophobic. In fact, fluorescent dyes may increase the molar mass of these short peptides by a mass corresponding to that of 3 (for fluorescein), 5 (for rhodamine) or even more amino acids. For example, as mentioned above, the nonapeptide RL9 is hardly internalized in CHO cells and has no cytotoxicity up to 20  $\mu\text{M}$ <sup>38, 48</sup>. In contrast, the Alexa-488 labeled RL9 is already cytotoxic at low  $\mu\text{M}$  concentrations. When the fluorescent peptide is incubated at a concentration slightly cytotoxic, it can be observed inside cells and model giant vesicles. When the concentration is reduced to non-cytotoxic one, the peptide is no longer detected in cells, showing that the use of fluorescent peptides can give way to false positive results in internalization studies. In addition, depending on its anchoring position on the peptide, the fluorescent dye can more or less affect the efficiency of CPP entry<sup>49</sup>.

We demonstrated that absolute quantification of internalized CPPs is also possible by fluorometry, using a protocol similar to the one established for MS quantification<sup>49</sup>: membrane-bound peptide is removed by protease treatment and cell are lysed before measuring peptide amounts in both cases<sup>49</sup>. Although the two techniques are totally different, results obtained by fluorometry and by mass spectrometry converge, for different cell lines and peptide sequences. Relative quantification by flow cytometry also merge with those obtained by fluorometry and mass spectrometry, but in a restricted range of peptide to cell ratio. This was not unexpected since the protocols used for mass spectrometry and fluorometry techniques are destructive for cells, and allow the accurate detection of the totality of the internalized peptide. In particular, in the case of fluorometry, the full fluorescence signal is recovered after cell lysis (absence of fluorescence quenching, controlled pH for prototropic and solvatochromic dyes, such as fluorescein). In contrast, flow cytometry, a non-intrusive technique like fluorescence imaging, is limited by the cell structure and organization: quenching processes and formation of non-fluorescent peptide species can indeed occur in the cell membrane and inside cells. For all techniques, we recommend to run in parallel cytotoxicity assays and when using flow cytometry to quantify fluorescent CPP internalization,

to test different peptide/cell ratios for consistency, to ensure the complete removal of membrane-bound species, and to consider potential quenching processes and formation of non-fluorescent peptide species (formation of aggregates, acidic pH)<sup>49</sup>.

### **Future direction - lessons from homeoproteins**

We described methods (Figure 5) and the complex study of membrane crossing of cell-penetrating peptides, a question that remains open in the field. One particular point we have not discussed in this Account relates to the lack of selective entry of CPPs in cells. This is obviously not the case for example for homeoproteins, these highly specialized transcription factors that transfer from cell to cell. Some homeoproteins show for instance selective entry into specific neuronal cells in the central nervous system of animals<sup>51</sup>. Since these proteins include very specialized and independent peptide domains with defined functions, we should take advantage of those to identify protein domains, that would help CPPs to target specifically cell-surface molecules and enhance their selectivity.

### **Biographical information**

**Dr. Astrid Walrant** obtained her Ph. D. in Chemistry in 2011 from the Université P. et M. Curie (Paris, France). She then joined the group of Jenny Gallop, at the Gurdon Institute and Biochemistry Department, University of Cambridge, (UK) as a postdoctoral researcher. She joined the Université P. et M. Curie as an Assistant Professor in 2014, at the Chemistry Department. Her research focuses on the analysis of the interactions of membrane active peptides and proteins with model and biological membranes.

**Dr. Sébastien Cardon** obtained two M.Sc. one in Organic Chemistry (2013) from the Université P. et M. Curie, and one in Biology (2014) from the Université Paris Diderot. During his masters, he worked on structure-activity relationships of antimicrobial peptides with Dr. Claire Lacombe, and on the residues involved in the selective transfer properties of the model enzyme FemXw with Dr. Matthieu Fonvielle. In October 2017, he obtained his Ph.D. on the specific role of GAGs on the structure and internalization properties of the homeoprotein Engrailed 2, under the supervision of Dr. Sandrine Sagan and Dr. Ludovic Carlier.

**Dr. Fabienne Burlina** obtained her Ph. D. in Chemistry in 1996 from the Université de Paris Sud (France). She then joined the group of M. J. Gait at the LMB (Cambridge, UK) as a post-doctoral fellow. Since 1999, she works in the Chemistry Department of the Université P. et M. Curie (Paris, France) as a CNRS researcher. Her current research focuses on the design and study of cell-penetrating peptides for the delivery of bioactive compounds. She is also interested in the development of ligation methodologies for the synthesis of bio-conjugates and proteins.

**Dr. Sandrine Sagan** obtained her Ph.D. (1991) in Molecular and Cellular Pharmacology from the Université P. et M. Curie (UPMC), Paris (France), at the Institut Jacques Monod. She pursued as a postdoctoral fellow at Salzburg research institute (Austria). In 1993, she joined the Chemistry Department of UPMC, where she is now heading a laboratory as a CNRS senior researcher. She has contributed structure-activity relationships in opioid, cannabinoid and tachykinin systems, photolabeling and mass spectrometry of membrane proteins, and is currently focused on the comprehensive analysis of the molecular mechanisms of entry of cell-penetrating peptides.

### **References**

1. Green, M.; Ishino, M.; Loewenstein, P.M. Mutational analysis of HIV-1 Tat minimal domain peptides: identification of trans-dominant mutants that suppress HIV-LTR-driven gene expression. *Cell*. 1989, 58, 215-223.
2. Vivès, E.; Brodin, P.; Lebleu, B. A truncated HIV-1 Tat protein basic domain rapidly translocates through the plasma membrane and accumulates in the cell nucleus. *J. Biol. Chem.* 1997, 272, 16010-16017.
3. Joliot, A.H.; Triller, A.; Volovitch, M.; Pernelle, C.; Prochiantz, A. Alpha-2,8-Polysialic acid is the neuronal surface receptor of antennapedia homeobox peptide. *New Biol.* 1991, 3, 1121-1134.

4. Derossi, D.; Joliot, A.H.; Chassaing, G.; Prochiantz, A. The third helix of the Antennapedia homeodomain translocates through biological membranes. *J. Biol. Chem.* 1994, 269, 10444-10450.
5. Copolovici, D.M.; Langel, K.; Eriste, E.; Langel, Ü. Cell-penetrating peptides: design, synthesis, and applications. *ACS Nano.* 2014, 8, 1972-1994.
6. Ruoslahti, E. Tumor penetrating peptides for improved drug delivery. *Adv. Drug Del. Rev.* 2017, 110, 3-12.
7. Eiríksdóttir, E.; Konate, K.; Langel, Ü.; Divita, G.; Deshayes, S. Secondary structure of cell-penetrating peptides controls membrane interaction and insertion. *Biochim. Biophys. Acta.* 2010, 1798, 1119-1128.
8. Bechara, C.; Pallerla, M.; Zaltsman, Y.; Burlina, F.; Alves, I.D.; Lequin, O.; Sagan, S. Tryptophan within basic peptide sequences triggers glycosaminoglycan-dependent endocytosis. *FASEB J.* 2013, 27, 738-749.
9. Bayer, P.; Kraft, M.; Ejchart, A.; Westendorp, M.; Frank, R.; Rösch, P. Structural studies of HIV-1 Tat protein. *J. Mol. Biol.* 1995, 247, 529-535.
10. Magzoub, M.; Eriksson, L.E.; Gräslund, A. Conformational states of the cell-penetrating peptide penetratin when interacting with phospholipid vesicles: effects of surface charge and peptide concentration. *Biochim. Biophys. Acta.* 2002, 1563, 53-63.
11. Esko, J.D.; Kimata, K.; Lindahl, U. Proteoglycans and sulfated glycosaminoglycans. In *Essentials of Glycobiology*; Varki, A., Cummings, R.D., Esko, J.D., Freeze, H.H., Stanley, P., Bertozzi, C.R., Hart, G.W., Etzler, M.E., Eds. 2nd edition. Cold Spring Harbor (NY): Cold Spring Harbor Laboratory Press, 2009; Chapter 16.
12. Iozzo, R.V. Turnover of heparan sulfate proteoglycan in human colon carcinoma cells. A quantitative biochemical and autoradiographic study. *J. Biol. Chem.* 1987, 262, 1888-1900.
13. van Meer G.; Voelker, D.R.; Feigenson, G.W. Membrane lipids: where they are and how they behave. *Nat. Rev. Mol. Cell Biol.* 2008, 9, 112-124.
14. Tkachenko, E.; Simons, M. Clustering induces redistribution of syndecan-4 core protein into raft membrane domains. *J. Biol. Chem.* 2002, 277, 19946-19951.
15. Binch, A.L.A.; Shapiro, I.M.; Risbud, M.V. Syndecan-4 in intervertebral disc and cartilage: Saint or synner? *Matrix Biol.* 2016, 52-54, 355-362.
16. Cullis, P.R.; De Kruijff, B. Lipid polymorphism and the functional roles of lipids in biological membranes. *Biochim. Biophys. Acta* 1979, 559, 399-420.
17. Mills, J.T.; Furlong, S.T.; Dawidowicz, E.A. Plasma membrane biogenesis in eukaryotic cells: translocation of newly synthesized lipid. *Proc. Natl. Acad. Sci. U.S.A.* 1984, 81, 1385-1388.
18. Aubry, S.; Burlina, F.; Dupont, E.; Delaroche, D.; Joliot, A.; Lavielle, S.; Chassaing, G.; Sagan, S. Cell-surface thiols affect cell entry of disulfide-conjugated peptides. *FASEB J.* 2009, 23, 2956-2967.
19. Aubry, S.; Aussedat, B.; Delaroche, D.; Jiao, C.Y.; Bolbach, G.; Lavielle, S.; Chassaing, G.; Sagan, S.; Burlina, F. MALDI-TOF mass spectrometry: a powerful tool to study the internalization of cell-penetrating peptides. *Biochim. Biophys. Acta.* 2010, 1798, 2182-2189.
20. Emi, N.; Kidoaki, S.; Yoshikawa, K.; Saito, H. Gene transfer mediated by polyarginine requires a formation of big carrier-complex of DNA aggregate. *Biochem. Biophys. Res. Commun.* 1997, 231, 421-424.
21. Mitchell, D.J.; Kim, D.T.; Steinman, L.; Fathman, C.G.; Rothbard, J.B. Polyarginine enters cells more efficiently than other polycationic homopolymers. *J. Pept. Res.* 2000, 56, 318-325.
22. Futaki, S.; Suzuki, T.; Ohashi, W.; Yagami, T.; Tanaka, S.; Ueda, K.; Sugiura, Y. Arginine-rich peptides. An abundant source of membrane-permeable peptides having potential as carriers for intracellular protein delivery. *J. Biol. Chem.* 2001, 276, 5836-5840.
23. Sakai, N.; Matile, S. Anion-mediated transfer of polyarginine across liquid and bilayer membranes. *J. Am. Chem. Soc.* 2003, 125, 14348-14356.
24. Rothbard, J.B.; Jessop, T.C.; Lewis, R.S.; Murray, B.A.; Wender, P.A. Role of membrane potential and hydrogen bonding in the mechanism of translocation of guanidinium-rich peptides into cells. *J. Am. Chem. Soc.* 2004, 126, 9506-9507.
25. Palm-Apergi, C.; Lorents, A.; Padari, K.; Pooga, M.; Hällbrink, M. The membrane repair response masks membrane disturbances caused by cell-penetrating peptide uptake. *FASEB J.* 2009, 23, 214-223.
26. Berlose, J.P.; Convert, O.; Derossi, D.; Brunissen, A.; Chassaing, G. Conformational and associative behaviours of the third helix of antennapedia homeodomain in membrane-mimetic environments. *Eur. J. Biochem.* 1996, 242, 372-386.

27. Wadia, J.S.; Stan, R.V.; Dowdy, S.F. Transducible TAT-HA fusogenic peptide enhances escape of TAT-fusion proteins after lipid raft macropinocytosis. *Nat. Med.* 2004, 10, 310-315.
28. Dunn, W.A.; Hubbard, A.L.; Aronson, N.N. Low-temperature selectively inhibits fusion between pinocytotic vesicles and lysosomes during heterophagy of asialofetuin-i-125 by the perfused-rat-liver. *J. Biol. Chem.* 1980, 255, 5971-5978.
29. Vercauteren, D.; Vandenbroucke, R.E.; Jones, A.T.; Rejman, J.; Demeester, J.; De Smedt, S.C.; Sanders, N.N.; Braeckmans, K. The use of inhibitors to study endocytic pathways of gene carriers: optimization and pitfalls. *Mol. Ther.* 2010, 18, 561-569.
30. Jiao, C.Y.; Delaroche, D.; Burlina, F.; Alves, I.D.; Chassaing, G.; Sagan, S. Translocation and endocytosis for cell-penetrating peptide internalization. *J. Biol. Chem.* 2009, 284, 33957-33965.
31. Alves, I.D.; Bechara, C.; Walrant, A.; Zaltsman, Y.; Jiao, C.Y.; Sagan, S. Relationships between membrane binding, affinity and cell internalization efficacy of a cell-penetrating peptide: penetratin as a case study. *PLoS One.* 2011;6(9):e24096.
32. Bechara, C.; Pallerla, M.; Zaltsman, Y.; Burlina, F.; Alves, I.D.; Lequin, O.; Sagan, S. Tryptophan within basic peptide sequences triggers glycosaminoglycan-dependent endocytosis. *FASEB J.* 2013, 27, 738-749.
33. Favretto, M.E.; Wallbrecher, R.; Schmidt, S.; van de Putte, R.; Brock, R. Glycosaminoglycans in the cellular uptake of drug delivery vectors - bystanders or active players? *J. Control. Release.* 2014, 180, 81-90.
34. Bechara, C.; Pallerla, M.; Burlina, F.; Illien, F.; Cribier, S.; Sagan, S. Massive glycosaminoglycan-dependent entry of Trp-containing cell-penetrating peptides induced by exogenous sphingomyelinase or cholesterol depletion. *Cell. Mol. Life Sci.* 2015, 72(4):809-820.
35. Jiao, C.Y.; Sachon, E.; Alves, I.D.; Chassaing, G.; Bolbach, G.; Sagan, S. Exploiting benzophenone photoreactivity to probe the phospholipid environment and insertion depth of the cell-penetrating peptide Penetratin in model membranes. *Angew. Chem. Int. Ed. Engl.* 2017, 56, 8226-8230.
36. Bechara, C.; Sagan, S. Cell-penetrating peptides: 20 years later, where do we stand? *FEBS Lett.* 2013, 587, 1693-1702.
37. Delaroche, D.; Aussedat, B.; Aubry, S.; Chassaing, G.; Burlina, F.; Clodic, G.; Bolbach, G.; Lavielle, S.; Sagan, S. Tracking a new cell-penetrating (W/R) nonapeptide, through an enzyme-stable mass spectrometry reporter tag. *Anal. Chem.* 2007, 79, 1932-1938.
38. Walrant, A.; Correia, I.; Jiao, C.Y.; Lequin, O.; Bent, E.H.; Goasdoué, N.; Lacombe, C.; Chassaing, G.; Sagan, S.; Alves, I.D. Different membrane behaviour and cellular uptake of three basic arginine-rich peptides. *Biochim. Biophys. Acta.* 2011, 1808, 382-393.
39. Walrant, A.; Vogel, A.; Correia, I.; Lequin, O.; Olausson, B.E.; Desbat, B.; Sagan, S.; Alves, I.D. Membrane interactions of two arginine-rich peptides with different cell internalization capacities. *Biochim. Biophys. Acta.* 2012, 1818, 1755-1763.
40. Burlina, F.; Sagan, S.; Bolbach, G.; Chassaing, G. Quantification of the cellular uptake of cell-penetrating peptides by MALDI-TOF mass spectrometry. *Angew. Chem. Int. Ed. Engl.* 2005, 44, 4244-4247.
41. Gonçalves, E.; Kitas, E.; Seelig, J. Binding of oligoarginine to membrane lipids and heparan sulfate: structural and thermodynamic characterization of a cell-penetrating peptide. *Biochemistry.* 2005, 44, 2692-2702.
42. Sagan, S.; Burlina, F.; Alves, I.D.; Bechara, C.; Dupont, E.; Joliot, A. Homeoproteins and homeoprotein-derived peptides: going in and out. *Curr. Pharm. Des.* 2013, 19, 2851-2862.
43. Christianson, H.C.; Belting, M. Heparan sulfate proteoglycan as a cell-surface endocytosis receptor. *Matrix Biol.* 2014, 35, 51-55.
44. Burlina, F.; Sagan, S.; Bolbach, G.; Chassaing, G. A direct approach to quantification of the cellular uptake of cell-penetrating peptides using MALDI-TOF mass spectrometry. *Nat. Protoc.* 2006, 1, 200-205.
45. Sagan, S.; Bechara, C.; Burlina, F. Study of CPP Mechanisms by Mass Spectrometry. *Methods Mol. Biol.* 2015, 1324, 107-121.
46. Aussedat, B.; Dupont, E.; Sagan, S.; Joliot, A.; Lavielle, S.; Chassaing, G.; Burlina, F. Modifications in the chemical structure of Trojan carriers: impact on cargo delivery. *Chem. Commun. (Camb).* 2008, 12, 1398-1400.
47. Bode, S.A.; Thévenin, M.; Bechara, C.; Sagan, S.; Bregant, S.; Lavielle, S.; Chassaing, G.; Burlina, F. Self-assembling mini cell-penetrating peptides enter by both direct translocation and glycosaminoglycan-dependent endocytosis. *Chem. Commun. (Camb).* 2012, 48, 7179-7181.

48. Walrant, A.; Matheron, L.; Cribier, S.; Chaignepain, S.; Jobin, M.L.; Sagan, S.; Alves, ID. Direct translocation of cell-penetrating peptides in liposomes: a combined mass spectrometry quantification and fluorescence detection study. *Anal. Biochem.* 2013, 438, 1-10.
49. Illien, F.; Rodriguez, N.; Amoura, M.; Joliot, A.; Pallerla, M.; Cribier, S.; Burlina, F.; Sagan, S. Quantitative fluorescence spectroscopy and flow cytometry analyses of cell-penetrating peptides internalization pathways: optimization, pitfalls, comparison with mass spectrometry quantification. *Sci. Rep.* 2016, 6, 36938.
50. Kauffman, W.B.; Fuselier, T.; He, J.; Wimley, W.C. Mechanism Matters: A Taxonomy of Cell Penetrating Peptides. *Trends Biochem Sci.* 2015, 40, 749-764.
51. Beurdeley, M.; Spatazza, J.; Lee, H.H.; Sugiyama, S.; Bernard, C.; Di Nardo, A.A.; Hensch, T.K.; Prochiantz, A. Otx2 binding to perineuronal nets persistently regulates plasticity in the mature visual cortex. *J. Neurosci.* 2012, 32, 9429-9437.

accepted manuscript

# Multicomponent Model for the Prediction of Nuclear Waste/Rare-Earth Extraction Processes

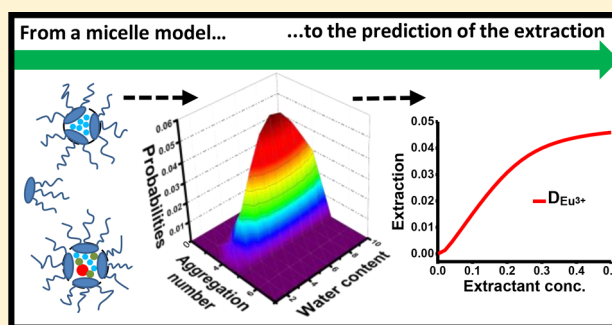
Mario Špadina,<sup>\*,†</sup> Klemen Bohinc,<sup>‡</sup> Thomas Zemb,<sup>†</sup> and Jean-François Duffrêche<sup>\*,†</sup>

<sup>†</sup>Institut de Chimie Séparative de Marcoule, Ecole Nationale Supérieure de Chimie de Montpellier, CEA/CNRS, Université de Montpellier, F-30207 Bagnols sur Ceze Cedex, France

<sup>‡</sup>Faculty of Health Sciences, University of Ljubljana, 1000 Ljubljana, Slovenia

**S** Supporting Information

**ABSTRACT:** We develop a minimal model for the prediction of solvent extraction. We consider a rare earth extraction system for which the solvent phase is similar to water-poor microemulsions. All physical molecular quantities used in the calculation can be measured separately. The model takes into account competition complexation, mixing entropy of complexed species, differences of salt concentrations between the two phases, and the surfactant nature of extractant molecules. We consider the practical case where rare earths are extracted from iron nitrates in the presence of acids with a common neutral complexing extractant. The solvent wetting of the reverse aggregates is taken into account via the spontaneous packing. All the water-in-oil reverse aggregates are supposed to be spherical on average. The minimal model captures several features observed in practice: reverse aggregates with different water and extractant content coexist dynamically with monomeric extractant molecules at and above a critical aggregate concentration (CAC). The CAC decreases upon the addition of electrolytes in the aqueous phase. The free energy of transfer of an ion to the organic phase is lower than the driving complexation. The commonly observed log–log relation used to determine the apparent stoichiometry of complexation is valid as a guideline but should be used with care. The results point to the fact that stoichiometry, as well as the probabilities of a particular aggregate, is dependent on the composition of the entire system, namely the extractant and the target solutes' concentrations. Moreover, the experimentally observed dependence of the extraction efficiency on branching of the extractant chains in a given solvent can be quantified. The evolution of the distribution coefficient of particular rare earth, acid, or other different metallic cations can be studied as a function of initial extractant concentration through the whole region that is typically used by chemical engineers. For every chemical species involved in the calculation, the model is able to predict the exact equilibrium concentration in both the aqueous and the solvent phases at a given thermodynamic temperature.



## INTRODUCTION

In the context of selective recovery of rare earth elements (REEs) or removal of lanthanides and actinides in nuclear waste processing, liquid–liquid extraction basically represents the first and only choice for the development of efficient large-scale processes.<sup>1,2</sup> These two overlapping fields, REEs recycling and nuclear waste processing, in fact constitute a major branch of hydrometallurgy. The importance of this branch is tightly linked to and influenced by industrial and the economic growth worldwide.<sup>2–5</sup>

REEs have a major role in sustaining a green, low-carbon economy. Their numerous applications include permanent magnets, lamp phosphors, batteries for hybrid cars, etc. However, use of REEs also puts importance on their recovery from production scraps and end-of-life products.<sup>1,4–6</sup> Extraction of lanthanides and actinides constitutes a challenge in the field of nuclear energy, as they represent the second stage of purification of spent fuel in fission reactors. In the French Alternative Energies and Atomic Energy Commission (CEA),

the implemented process involves the separation of plutonium and uranium in the first stage (the PUREX process) and co-extraction of the remaining lanthanides and actinides in the second stage (the DIAMEX process).<sup>7,8</sup>

An efficient liquid–liquid extraction process requires a particular extractant molecule dissolved in a solvent, which in turn forms a sort of weak complex with the target metal cation.<sup>9</sup> In the case of DIAMEX process, the extractant is DMDOHEMA (*N,N'*-dimethyl-*N,N'*-dioctyl-2-(2-hexyloxyethyl)malonamide).<sup>7</sup> The extractant molecules tend to self-assemble into reverse aggregates of various compositions. The compositions depend on the type of the extractant, the extracted solute, the temperature, pH, the salt concentration in the aqueous phase, and the type of the organic solvent.<sup>10–13</sup>

**Received:** May 27, 2018

**Revised:** July 18, 2018

**Published:** August 6, 2018

Over the years, various liquid–liquid extraction processes for different systems have been optimized and augmented on the industrial scale. Along with the well-understood experimental methods, a few thermodynamic models have been proposed.<sup>14,15</sup> Still, most of the models are based on the principle that all possible equilibria are established and then fitting over the experimental data is employed.<sup>16</sup> As a result, a set of apparent equilibrium constants and adjusted parameters is obtained.<sup>1,17,18</sup> Often there are more adjusted parameters than observable quantities. Even though satisfactory fits are usually obtained, the question arises whether such models could, in fact, be generalized for different extractants. Moreover, water molecules and organic solvent are neglected within the law of mass action.<sup>19</sup> By neglecting a solvent's influence, the obtained apparent ion transfer constants do not depend on the branching of the extractant's alkyl chains, which is completely opposite to experimental observations. Note also that the majority of the models are made to reproduce results of simple laboratory-size systems (which take into account only a few components).

In order to acquire insight into the forces that influence the aggregation process and the overall extraction, we propose a model derived from statistical thermodynamics coupled with ideas and models of molecular self-assembly of the extractant molecules. Our goal is to propose a new methodology with a minimal number of adjusted parameters. Moreover, the parameters themselves ought to reflect the molecular nature of reverse aggregate constituents. Within this paper, we aim to show how our model captures some of the relevant properties of systems formulated from an efficient extraction. An example will be made using the practical case of multicomponent extraction for acidic media. The system in study is composed of heptane solvent containing DMDOHEMA extractant and an aqueous phase containing three extracted solutes, namely, nitric acid, europium(III) nitrate, and iron(III) nitrate. We will also show how the choice of geometrical parameters, widely used to describe curved interfaces, influences the microscopic picture of reverse micelles. Finally, a quantitative description of the reversible extraction formulations will be provided.

## THEORY

**Free Energy of the Reverse Micelle.** The model system consists of two phases in contact, namely, the aqueous solution containing multiple ion species and the organic phase containing monomeric extractant molecules (DMDOHEMA) and self-assembled water-in-oil reverse micelles (i.e., the aggregates). We keep this historical name even though we always have a minimum of three components, namely, the water, the extractant, and the solvent. All species are in thermodynamic equilibrium. The aqueous solution represents the brine, whereas the organic phase is the solvent phase in the DIAMEX process. A model system is applicable to any hydrometallurgical process which utilizes an uncharged extractant. It must be noted that hydrophilicity in terms of partitioning of the DMDOHEMA extractant in aqueous phase is not taken into account. It was shown that, globally, the effect is small for uncharged chelating and solvating extractants.<sup>20,21</sup> The aggregates are considered as spheres with two distinct parts. The outer part is assumed to be a layer of extractant molecule chains with the average length  $l_{\text{chain}}$ . The inner part, or the core of the aggregate, consists of extractant polar head groups immersed in the droplet of an aqueous solution of ions that takes up the remaining volume,  $V_{\text{core}}$ .

The free energy of an aggregate of particular composition,  $F_{\text{Agg}_{N_w, N_i, N_1}}$ , can be written as follows:

$$F_{\text{Agg}_{N_w, N_i, N_1}} = F_{\text{chain}} + F_{\text{core}} \quad (1)$$

where  $F_{\text{chain}}$  is the free energy associated with the layer of extractant molecules (in short, the chain term) and  $F_{\text{core}}$  is the free energy of the core of the aggregate, defined as

$$F_{\text{core}} = F_{\text{droplet}} + F_{\text{complex}} \quad (2)$$

$F_{\text{droplet}}$  is the free energy of a droplet of aqueous electrolyte solution, and  $F_{\text{complex}}$  is the term which describes interactions between cations and extractant head groups.  $F_{\text{droplet}}$  and  $F_{\text{complex}}$  will be discussed later in this section.  $F_{\text{chain}}$  has been taken into account in an already well-established approach through the relation<sup>14</sup>

$$F_{\text{chain}} = \frac{N_1}{2} \kappa^* (p - p_0)^2 \quad (3)$$

where  $N_1$  is the number of extractant molecules assembled into a reverse aggregate,  $\kappa^*$  represents the generalized bending constant for one extractant molecule in the extractant film,  $p$  is the packing parameter of the extractant molecule, and  $p_0$  is the intrinsic spontaneous packing parameter for a certain type of extractant.<sup>22–24</sup> For a fixed chain length, the packing parameter can be written in an explicit form as<sup>25–27</sup>

$$p = 1 + \frac{l_{\text{chain}}}{R_{\text{core}}} + \frac{1}{3} \frac{l_{\text{chain}}^2}{R_{\text{core}}^2} \quad (4)$$

where the radius of the core is

$$R_{\text{core}} = \sqrt[3]{\frac{3}{4\pi} \left( \sum_i N_i V_{m,i} + N_w V_{m,w} + N_1 V_{m,1} \right)} \quad (5)$$

and  $N_i$ ,  $N_w$ , and  $N_1$  are respectively the numbers of ions, water molecules, and extractant head groups that constitute the core of the aggregate, whereas  $V_{m,i}$ ,  $V_{m,w}$ , and  $V_{m,1}$  are respectively the specific molar volumes of ions, water molecules, and extractant head groups. The molar volumes are taken from the literature.<sup>28</sup>

To calculate  $F_{\text{core}}$ , first we need to calculate the free energy of a single droplet of aqueous solution,  $F_{\text{droplet}}$ , immersed in a medium characterized with a low dielectric constant. The partition function  $\tilde{Z}$  in a canonical ensemble for a single droplet of an aqueous solution of ions can be written as<sup>29,30</sup>

$$\tilde{Z} = \frac{1}{N_w! \prod_i N_i!} \frac{1}{h^{3N_w} \prod_i h^{3N_i}} \times \int \dots \int d\mathbf{r}^{N_w} d\mathbf{r}^{N_i} d\mathbf{p}^{N_w} d\mathbf{p}^{N_i} e^{-\beta(V + \sum_k \frac{\mathbf{p}_k^2}{2m_k})} \quad (6)$$

where the index  $k$  sums over the total number of particles (ions and water molecules) in the droplet,  $h$  is Planck's constant,  $\mathbf{r}_k$  and  $\mathbf{p}_k$  are respectively the position and momentum of each particle in the droplet,  $\beta$  is defined as  $\beta = 1/k_B T$ , where  $k_B$  is the Boltzmann constant and  $T$  is the thermodynamic temperature,  $m_k$  is the mass of the  $k$ -th particle, and  $V$  is the interacting potential among particles. The factorials in the denominator of eq 6 account for the indistinguishability of particles. For the sake of simplicity, we consider all particles as spherical objects with no internal degrees of freedom (as

sketched in Figure 1). In such a formulation, the integral of eq 6 over momenta of the particles gives

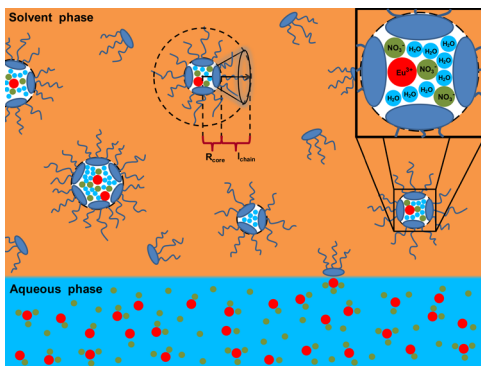


**Figure 1.** Schematic representation of the extraction process. Various types of aggregates are present in the solvent, and their probability at equilibrium is determined by the composition of their cores. Considering the surfactant nature of the extractant, the interface is at least partially covered by the extractant molecules (not shown here).

$$\tilde{Z} = \frac{1}{N_w! \prod_i N_i!} \frac{1}{\Lambda_w^{3N_w} \prod_i \Lambda_i^{3N_i}} \times \int \dots \int d\mathbf{r}^{N_w} d\mathbf{r}^{N_i} e^{-\beta V} \quad (7)$$

where  $\Lambda_w$  and  $\Lambda_i$  are the effective de Broglie thermal wavelengths of water molecules and ions, respectively. Equation 7 holds for large numbers of particles. In contrast to such conditions, our droplet is composed of typically up to 10 particles, with small variation depending on the composition of the polar core. Therefore,  $\tilde{Z}$  needs to be corrected for such a small number of particles. If Stirling's approximation is written as  $N! \approx N^N e^{-N}$ , then

$$\tilde{Z}_{\text{approx}} = \frac{N_w^{N_w} e^{-N_w} \prod_i N_i^{N_i} e^{-N_i}}{N_w! \prod_i N_i!} \tilde{Z} \quad (8)$$

where  $\tilde{Z}_{\text{approx}}$  is the canonical partition function for a droplet of aqueous electrolyte solution, corrected for the small number of particles. Free energy in a canonical ensemble can be evaluated through the relation  $F_{\text{droplet}} = -k_B T \ln \tilde{Z}_{\text{approx}}$  and the following expression is obtained:

$$F_{\text{droplet}} = k_B T \ln \frac{N_w! \prod_i N_i!}{N_w^{N_w} e^{-N_w} \prod_i N_i^{N_i} e^{-N_i}} - k_B T \ln \tilde{Z} \quad (9)$$

where  $F_{\text{droplet}}$  denotes the free energy of the droplet made out of a small number of particles. After applying logarithm rules and sorting all the terms, we end up with the following expression:

$$F_{\text{droplet}} = k_B T \ln \left( N_w! \prod_i N_i! \right) - k_B T \left( N_w \ln N_w + \sum_i N_i \ln N_i - N_w - \sum_i N_i \right) - k_B T \ln \tilde{Z} \quad (10)$$

The first terms of the right side of eq 10 represent a correction of the partition function for a small number of particles, whereas the last term,  $k_B T \ln \tilde{Z}$ , represents the free energy  $F_{\text{elect}}$  of the equivalent system in the bulk, where Stirling's approximation is applicable. Since we consider the condensed phase, namely, a liquid, we can equalize  $F_{\text{elect}} \approx G_{\text{elect}}$  where the Gibbs energy of the electrolyte solution can be written as

$$G_{\text{elect}} = N_w \mu_w^{\text{org}} + \sum_i N_i \mu_i^{\text{org}} \quad (11)$$

where  $\mu_w^{\text{org}}$  and  $\mu_i^{\text{org}}$  are respectively chemical potentials of water molecules and ions confined in the core of the aggregate.<sup>31</sup> Within this paper we consider only ideal aqueous solutions both in the core of the aggregate and in the aqueous phase with both activity and osmotic coefficients equal to 1.<sup>31</sup> Furthermore, an approximation has been made that the standard chemical potentials of ions and water confined inside this droplet are the same as the ones in aqueous solution in contact, i.e., the same reference state is understood.<sup>32</sup> Therefore, we obtain

$$\mu_i^{\text{org}} = \mu_i^\circ + k_B T \ln \left( \frac{m_i^{\text{org}}}{m_i^\circ} \right) \quad (12)$$

and

$$\mu_w^{\text{org}} = \mu_w^\circ - k_B T \frac{\sum_i x_i^{\text{org}}}{x_w^{\text{org}}} = \mu_w^\circ - k_B T \frac{\sum_i N_i}{N_w} \quad (13)$$

where  $\mu_i^{\text{org}}$ ,  $\mu_w^{\text{org}}$ ,  $\mu_i^\circ$ ,  $\mu_w^\circ$ ,  $m_i^{\text{org}}$ ,  $m_i^\circ$ ,  $x_i^{\text{org}}$ , and  $x_w^{\text{org}}$  are respectively the chemical potentials of ions and water in the core of the aggregate, the standard chemical potentials of ions and water in the core of the aggregate, the molal concentration of ions in the core, the molal concentration of ions at standard state, and the mole fraction of ions and water in the core. Equation 13 is the consequence of eq 12 when the Gibbs–Duhem relation is used.

In order to calculate the free energy of the core,  $F_{\text{core}}$ , we still need to include the complexation free energy term,  $F_{\text{complex}}$ . The complexation energy per particle,  $E_{0,\text{Cat}}$ , is defined as a favorable interaction that lowers the potential energy of the system, thus benefiting the extraction. It takes into account the first-sphere interactions between extractant head groups and solvated ions.<sup>14</sup> It typically represents the bond energy measured in the EXAFS measurements.<sup>33,34</sup> Now we can rewrite the corrected partition function  $\tilde{Z}_{\text{approx}}$  in the following way:

$$\tilde{Z}_{\text{approx}} = \frac{N_w! \prod_i N_i!}{N_w^{N_w} e^{-N_w} \prod_i N_i^{N_i} e^{-N_i}} \frac{1}{N_w! \prod_i N_i!} \frac{1}{\Lambda_w^{3N_w} \prod_i \Lambda_i^{3N_i}} \times \int \dots \int d\mathbf{r}^{N_w} d\mathbf{r}^{N_i} e^{-\beta(V - N_{\text{Cat}} E_{0,\text{Cat}})} \quad (14)$$

where  $N_{\text{Cat}}$  depicts the number of ions that are interacting with the extractant head groups (with appropriate energy  $E_{0,\text{Cat}}$ ). Since  $e^{\beta N_{\text{Cat}} E_{0,\text{Cat}}}$  is a constant term, it can be extracted from the integral. We obtain

$$\tilde{Z}_{\text{approx}} = e^{\beta N_{\text{Cat}} E_{0,\text{Cat}}} \frac{N_w^{N_w} e^{-N_w} \prod_i N_i^{N_i} e^{-N_i}}{N_w! \prod_i N_i!} \tilde{Z} \quad (15)$$

As there are multiple head groups available to interact with the “complexing” particle, the actual number of microstates scales with the multiplication factor  $N_{\text{complex}}$  within the partition function.  $N_{\text{complex}}$  takes into account all possible configurations of interacting extractant head groups and complexing particles. If we assume that every particle interacts with two head groups, then  $N_{\text{complex}}$  can be written as<sup>35,36</sup>

$$N_{\text{complex}} = \frac{N_1!}{(N_1 - 2N_{\text{Cat}})!} \frac{1}{2^{N_{\text{Cat}}}} \quad (16)$$

Note that the denominator in eq 16 does not contain a factorial for indistinguishability of the complexed particle, since it has already been included in the expression for  $\tilde{Z}_{\text{approx}}$ . The term  $2^{N_{\text{Cat}}}$  in the denominator accounts for the swap of two head groups to prevent double counting of the same configurations. Now the free energy of the core of the aggregate can be written as

$$F_{\text{core}} = -k_B T \ln(N_{\text{complex}} \tilde{Z}_{\text{approx}}) \quad (17)$$

which gives

$$F_{\text{core}} = -k_B T \ln N_{\text{complex}} - N_{\text{Cat}} E_{0,\text{Cat}} + F_{\text{droplet}} \quad (18)$$

Therefore, the complexation free energy term (recall eq 2) is

$$F_{\text{complex}} = -k_B T \ln N_{\text{complex}} - N_{\text{Cat}} E_{0,\text{Cat}} \quad (19)$$

We can conclude that  $F_{\text{complex}}$  consists of configuration entropy term  $-k_B T \ln N_{\text{complex}}$  and the internal energy term described as  $-N_{\text{Cat}} E_{0,\text{Cat}}$ . Indeed, this was a desired outcome when we defined  $F_{\text{complex}}$  in eq 2 and implemented the additional stabilizing potential  $E_{0,\text{Cat}}$  in eq 14.

When all terms from the expressions for  $F_{\text{core}}$  and  $F_{\text{chain}}$  are summed, the free energy of the aggregate of particular composition  $F_{\text{Agg}_{N_w, N_i, N_1}}$  is obtained (eq 1). The whole expression can be found in Appendix A. In fact,  $F_{\text{Agg}_{N_w, N_i, N_1}}$  is by definition the standard chemical potential,  $\mu_{\text{Agg}_{N_w, N_i, N_1}}^\circ$ , of the reverse micelle in the particular organic solvent (recall that the partition function was written for a single droplet of an aqueous solution with complexation).<sup>37</sup> Therefore, we can write

$$\mu_{\text{Agg}_{N_w, N_i, N_1}}^\circ = F_{\text{Agg}_{N_w, N_i, N_1}} \quad (20)$$

**Special Case of Pure Water Extraction.** The derivation so far was concerned with aggregates containing an electrolyte in the core. When only water molecules are present in the core, i.e., when we consider a pure phase, the corrected partition function,  $\tilde{Z}_{\text{pure},w}$  of such a system reduces to

$$\tilde{Z}_{\text{pure},w} = \frac{N_w!}{N_w^{N_w} e^{-N_w}} \frac{1}{N_w! \Lambda_w^{3N_w}} \int \dots \int d\mathbf{r}^{N_w} e^{-\beta V_{\text{pure},w}} \quad (21)$$

where  $V_{\text{pure},w}$  is the potential between water molecules. The free energy of the pure water droplet is then

$$F_{\text{droplet}} = k_B T \ln(N_w!) - N_w k_B T (\ln N_w - 1) + N_w \mu_w^{\text{org}} \quad (22)$$

which is equal to

$$F_{\text{droplet}} = k_B T \ln(N_w!) - N_w k_B T (\ln N_w - 1) + N_w \mu_w^\circ \quad (23)$$

In the absence of all terms describing the complexation,  $F_{\text{core}}$  is equal to  $F_{\text{droplet}}$ , whereas  $F_{\text{chain}}$  is calculated in the same manner as for the case with the ions present. It is obvious that addition of an electrolyte imposes much greater complexity in the system.

**Global Equilibrium.** Within this model we consider equilibria between an aggregate in the organic phase (solvent) and its constituents, namely, extractant molecules, and solvent, ions, and water molecules in the aqueous phase. We can write the law of mass action as

$$N_w \times W + \sum_i N_i \times I_i + N_1 \times \bar{L} \rightleftharpoons \overline{A_{N_w, N_i, N_1}} \quad (24)$$

where  $W$ ,  $I_i$ ,  $\bar{L}$ , and  $\overline{A_{N_w, N_i, N_1}}$  are respectively symbols for the water, ions in an aqueous phase, and extractant and aggregate in a solvent. Note that since DMDOHEMA is a neutral extractant, the cation is always transferred from aqueous phase to solvent along with an appropriate number of nitrate anions ( $\text{NO}_3^-$ ) to balance the charge. Salt molecules considered within this work are  $\text{HNO}_3$ ,  $\text{Eu}(\text{NO}_3)_3$ , and  $\text{Fe}(\text{NO}_3)_3$ . The chemical potentials of species involved in the chemical reaction described by eq 24 can be written as

$$\mu_{A_{N_w, N_i, N_1}} = \mu_{A_{N_w, N_i, N_1}}^\circ + k_B T \ln \left( \frac{c_{A_{N_w, N_i, N_1}}}{c^\circ} \right) \quad (25)$$

$$\mu_i = \mu_i^\circ + k_B T \ln \left( \frac{c_i}{c^\circ} \right) \quad (26)$$

$$\mu_i^{\text{aq}} = \mu_i^\circ + k_B T \ln \left( \frac{m_i^{\text{aq}}}{m_i^\circ} \right) \quad (27)$$

$$\mu_w^{\text{aq}} = \mu_w^\circ - k_B T \frac{\sum_i x_i^{\text{aq}}}{x_w^{\text{aq}}} \quad (28)$$

where  $\mu_{A_{N_w, N_i, N_1}}$ ,  $\mu_i$ ,  $\mu_i^\circ$ ,  $c_{A_{N_w, N_i, N_1}}$ ,  $c_i$ , and  $c^\circ$  are respectively the chemical potentials, the standard chemical potentials, and the concentrations at standard state of the aggregates and the extractant in a solvent.  $\mu_i^{\text{aq}}$ ,  $m_i^{\text{aq}}$ ,  $\mu_w^{\text{aq}}$ ,  $x_i^{\text{aq}}$ , and  $x_w^{\text{aq}}$  are respectively the chemical potentials and the molal concentration of ions, the chemical potential of water, and the mole fractions of ions and water in the aqueous phase. Equation 28 is the consequence of eq 27 when the the Gibbs–Duhem relation is used. To complete the calculation we need to write the law of mass action (eq 24) in terms of chemical potentials of all involved species:

$$\mu_{A_{N_w, N_i, N_1}} = N_1 \mu_1 + N_w \mu_w^{\text{aq}} + \sum_i N_i \mu_i^{\text{aq}} \quad (29)$$

which is equal to

$$\begin{aligned} \mu_{A_{N_w, N_i, N_1}}^\circ + k_B T \ln \left( \frac{c_{A_{N_w, N_i, N_1}}}{c^\circ} \right) = \\ N_w \mu_w^\circ - N_w k_B T \frac{\sum_i x_i^{\text{aq}}}{x_w^{\text{aq}}} + \sum_i N_i \mu_i^\circ \\ + k_B T \sum_i N_i \ln \left( \frac{m_i^{\text{aq}}}{m_i^\circ} \right) + N_1 \mu_1^\circ + N_1 k_B T \ln \left( \frac{c_1}{c^\circ} \right) \end{aligned} \quad (30)$$

At this point, it is convenient to define

$$\mu_{A_{N_w, N_i, N_1}}^{\circ''} = \mu_{A_{N_w, N_i, N_1}}^{\circ} - N_w \mu_w^{\text{org}} - \sum_i N_i \mu_i^{\text{org}} \quad (31)$$

where  $\mu_{A_{N_w, N_i, N_1}}^{\circ''}$  is the reduced standard chemical potential of the aggregate, obtained by subtracting the chemical potentials of ions and water confined in the core from  $\mu_{A_{N_w, N_i, N_1}}^{\circ}$ .  $\mu_{A_{N_w, N_i, N_1}}^{\circ''}$  still contains all the other terms, namely, the chain, the complexation, and terms for the correction for a small number of particles. After inserting eq 31 into eq 30, the standard chemical potentials of ions and water cancel out, and the following expression is obtained:

$$\begin{aligned} \mu_{A_{N_w, N_i, N_1}}^{\circ''} - N_w k_B T \frac{\sum_i N_i}{N_w} + k_B T \sum_i N_i \ln \left( \frac{m_i^{\text{org}}}{m_i^{\circ}} \right) \\ + k_B T \ln \left( \frac{c_{A_{N_w, N_i, N_1}}}{c^{\circ}} \right) = -N_w k_B T \frac{\sum_i x_i^{\text{aq}}}{x_w^{\text{aq}}} \\ + k_B T \sum_i N_i \ln \left( \frac{m_i^{\text{aq}}}{m_i^{\circ}} \right) + N_i \mu_i^{\circ} + N_i k_B T \ln \left( \frac{c_i}{c^{\circ}} \right) \end{aligned} \quad (32)$$

After some rearrangement of eq 32, multiplying with  $\beta$ , and exponentiation of the whole expression, we obtain

$$c_{A_{N_w, N_i, N_1}} = D c_i^{N_i} \quad (33)$$

where  $D$  is defined as

$$\begin{aligned} D = \exp \left( -\beta \mu_{A_{N_w, N_i, N_1}}^{\circ''} + \sum_i N_i \ln \left( \frac{m_i^{\text{aq}}}{m_i^{\text{org}}} \right) \right) \\ + N_w \left( \frac{\sum_i x_i^{\text{org}}}{x_w^{\text{org}}} - \frac{\sum_i x_i^{\text{aq}}}{x_w^{\text{aq}}} \right) + \beta N_i \mu_i^{\circ} \left( \frac{1}{c^{\circ}} \right)^{N_i - 1} \end{aligned} \quad (34)$$

To satisfy the law of mass action, the polynomial of degree  $l$  (eq 33) needs to be solved for any composition of the aggregate. The equilibrium concentration of extractant in the system,  $c_l$ , is the root of the polynomial of degree  $l$ . Furthermore, the system needs to be solved in such a way that the following conditions are satisfied:

$$c_1^{\text{tot}} = \sum_{\text{wli}} N_i c_{A_{N_w, N_i, N_1}} + c_1 \quad (35)$$

$$n_i^{\text{tot}} = n_i^{\text{org}} + n_i^{\text{aq}} \quad (36)$$

where  $c_1^{\text{tot}}$  and  $n_i^{\text{tot}}$  are respectively the total or the “initial” molar concentration of extractant and mole number of each ion species in the system. Both quantities are inputs of the model. The sum goes over all possible configurations of the aggregate.

To conclude this section it is worth noting that, instead of concentrations at equilibrium, aggregates will be described through their probabilities, since normalized quantities are easier to discuss. The equilibrium aggregate probability,  $P(w, l, i)$ , is defined as

$$P(w, i, l) = \frac{c_{A_{N_w, N_i, N_1}}}{\sum_{\text{wil}} c_{A_{N_w, N_i, N_1}}} \quad (37)$$

where  $c_{A_{N_w, N_i, N_1}}$  is the equilibrium concentration of the aggregate with a particular composition. The sum in the denominator goes over all possible aggregate concentrations.

## RESULTS AND DISCUSSION

**Input for the Model.** In order to perform the calculations, we need a certain set of measurable quantities as inputs for the model. We require the molar volumes of water, acid, salts, and extractant head groups ( $V_{m,w}$ ,  $V_{m,i}$ ,  $V_{m,l}$ ).<sup>28</sup> The length of the extractant molecule chains averaged of all conformations (i.e., the average length),  $l_{\text{chain}}$ , is also needed to perform the calculations.  $l_{\text{chain}}$  can be assessed through a combination of small-angle neutron scattering (SANS) and small-angle X-ray scattering (SAXS) pattern fits.<sup>38</sup>  $l_{\text{chain}}$  of DMDOHEMA molecule chains can also be calculated with molecular dynamics simulations. A recent study showed that results of simulations with explicit *n*-heptane solvent are in agreement with the experiments.<sup>27</sup>  $l_{\text{chain}}$  used for our model equals 9.6 Å, and it corresponds to typically 80% of fully stretched chain length. The length of the extractant molecule chains is considered not to change for different compositions of the core of the aggregate.

Within this study, the solvent is not included explicitly in the law of mass action, but it is still indirectly taken into account through the  $l_{\text{chain}}$  value used for the calculation. The influence of penetrating and non-penetrating solvents on the overall extraction process can therefore easily be included in this model.<sup>39</sup>

Along with measurable quantities, we need to specify the system in terms of initial concentrations of the species, namely, extractant molar concentration,  $c_1^{\text{tot}}$ , and ion molal concentrations,  $m_i^{\text{tot}}$ .

Beside measurable quantities and initial composition of the system, our model requires a set of parameters, namely, the standard chemical potential of monomeric extractant  $\mu_i^{\circ}$ , the spontaneous packing parameter  $p_0$ , the rigidity constant  $\kappa^*$ , and the complexation parameter  $E_{0,\text{Cat}}$  for solutes (except water) that can be extracted into the solvent phase. Among these values, only  $\mu_i^{\circ}$  is accessible by experiments.  $p_0$  and  $\kappa^*$  can generally be assessed by fitting a three-component phase diagram.<sup>40</sup> The procedure for adjusting the parameters and more detailed discussion about its properties are presented in the next section.

In calculations, the upper limit of both water and extractant molecules was set to  $N_w = N_l = 10$ . Our model is self-consistent, so values of  $N_w$  and  $N_l$  higher than 10 are not required (see next section). Moreover, these intervals represent what is typically observed in the vapor pressure osmometry measurements and in the fits of the SAXS/SANS patterns.<sup>18,41</sup> The complexation term  $F_{\text{complex}}$  (eq 19) is added under the condition that every extracted acid or salt molecule requires at least four extractant molecules to assemble the aggregate; therefore, we impose the rule  $N_{l,\text{min}} = 4N_{\text{Cat}}$ .

It is also important to emphasize that our model is made entirely for the case of spherical micelles, meaning that quantitative interpretation is possible for systems up to  $c_{l,\text{initial}} = 0.605 \text{ mol dm}^{-3}$  of DMDOHEMA (where worm-like micelles usually do not exist) and up to  $0.5 \text{ mol dm}^{-3}$   $\text{Eu}(\text{NO}_3)_3$  concentration (before the experimentally observed formation of the third phase occurs).<sup>42</sup>

**Model Parameters.** This part of the paper is dedicated to adjusting the model parameters and to the study of their influence on the properties of extraction systems. The model parameters ( $\kappa^*$ ,  $p_0$ ,  $\mu_i^{\circ}$ , and  $E_{0,\text{Cat}}$ ) were adjusted in such a manner that the three crucial conditions were satisfied. The first two conditions are, in fact, the experimentally observed

properties of reverse aggregates and extraction systems. The first condition deals with the composition of the aggregates in terms of aggregation number and water content, whereas the second condition ensures that the calculated critical aggregate concentration (CAC) is in accordance with the experimentally observed one. The third condition has more to do with the numerical nature of the calculation. The method needs to be self-consistent, and all results ought to be invariant to the choice of an upper limit of  $N_i$ ,  $N_w$ , and  $N_i$  used in calculations.

By satisfying these three crucial conditions, we end up with a small domain of possible sets of parameters, which means that the predicting power of the model is greatly enhanced. The prediction of an extraction process for various species is then a consequence of satisfying those conditions.

Note that the parametrization has been done step-by-step, which means that  $\kappa^*$ ,  $p_0$ , and  $\mu_i^0$  are adjusted for the extraction of water and are therefore considered fixed in later fitting of  $E_{0,Cat}$  for each solute. This is the only way to preserve reproducibility.

Before discussing the importance of a proper value of  $p_0$  used in the calculations, we need to study the dependence of the packing parameter  $p$  on aggregate compositions within the framework the concept used (eq 3). We have already stated that the average chain length,  $l_{chain}$ , is considered as a constant whatever the composition of the polar core of the aggregate. With such an approximation, the packing parameter  $p$  can be calculated using eq 4. Figure 2a shows the map of calculated  $p$

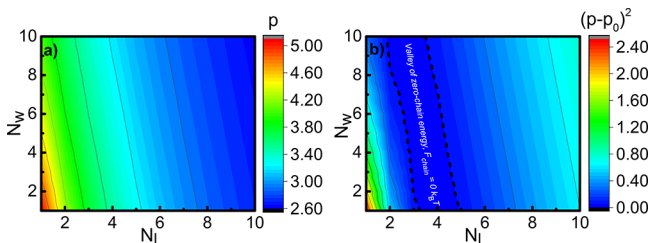


**Figure 2.** (a) Calculated packing parameter  $p$  as a function of the composition of the core of the aggregate (i.e., map of packing parameter for the reverse micelle). (b) Squared difference between calculated parameter  $p$  and spontaneous packing parameter  $p_0 = 3.5$  as a function of composition of the core of the aggregate. In both figures the core contains one salt molecule, namely  $\text{Eu}(\text{NO}_3)_3$ ,  $N_i$  depicts the number of extractant molecules (the aggregation number), and  $N_w$  depicts the number of water molecules present in the core (the water content).

as a function of the composition of the core of the aggregate when one salt molecule, namely  $\text{Eu}(\text{NO}_3)_3$ , is present inside. Note again that these values are a consequence of  $l_{chain} = 9.6 \text{ \AA}$  (heptane solvent). The different solvent would imply use of a different  $l_{chain}$  value, thus changing the map of calculated  $p$ . An important feature that can be seen in Figure 2a is that  $p$  asymptotically approaches a value  $p \approx 2.6$  for the high aggregation numbers,  $N_i$ , and the water molecule content,  $N_w$ . Note that if we were to calculate  $p$  for a very large number of extractant and water molecules (when  $N_i, N_w \rightarrow +\infty$ ),  $p$  would approach a value of 1 (eq 4), which means that, by huge swelling of the aggregate, we would end up in the lamellar phase (plane-like structure).<sup>43</sup>

Since  $F_{chain}$  is a function of  $p$  (eq 3), obviously it is important to use a proper value of spontaneous packing parameter  $p_0$  for the calculation.  $p_0$  describes the position of the “chain energy valley”, where  $F_{chain}$  is close to 0 or sufficiently small to allow

the formation of the aggregates. Consequently, the calculated equilibrium aggregate probabilities will be affected by the choice of  $p_0$ .

Equation 3 represents a simple harmonic approximation of the potential of mean force.<sup>27</sup> Therefore, it is convenient to study the squared differences between calculated  $p$  (each  $p$  corresponds to a particular composition of the core of an aggregate) and  $p_0$ , as plotted in Figure 2b. Figure 2b shows  $(p - p_0)^2$  calculated for  $p_0 = 3.5$ . The calculations have also been made with  $p_0 = 2.5$  and 3. The results of these calculations are presented in Figures S1 and S2 in the Supporting Information. It is worth mentioning that, even though the potential well is not perfectly symmetrical with respect to  $p_0$ , the approach is still quite suitable for the description of  $F_{chain}$  and provides acceptable results.<sup>44–46</sup>

When  $p_0 = 3.5$ , the preferred compositions correspond to four extractant molecules, and the number of water molecules varies between 1 and 7, depending on the type of solute present inside the core (Figure 3). This outcome of the model

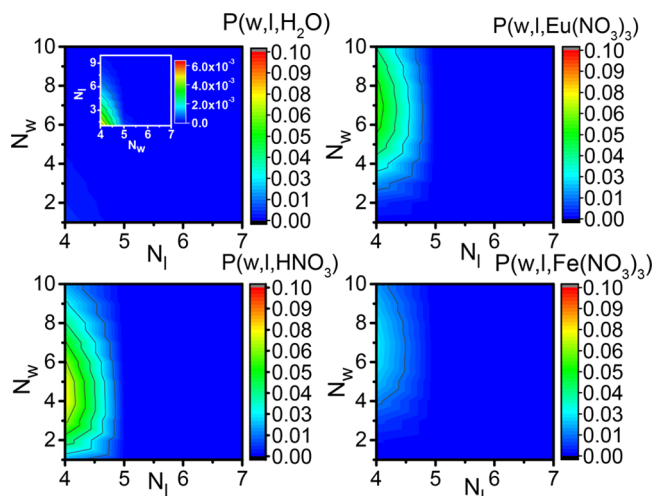


**Figure 3.** Calculated equilibrium aggregate probabilities as a function of the composition of the core of the aggregate.  $N_i$  depicts number of extractant, whereas  $N_w$  depicts number of water molecules present in the core. Scaled results of the upper left figure are shown in its inset. The model parameters are  $p_0 = 3.5$ ,  $\kappa^* = 16 k_B T$  per extractant molecule,  $\mu_i^0 = 2.5 \text{ kJ/mol}$ ,  $E_{0,\text{HNO}_3} = 5 k_B T$ ,  $E_{0,\text{Fe}(\text{NO}_3)_3} = 13 k_B T$ , and  $E_{0,\text{Eu}(\text{NO}_3)_3} = 15.6 k_B T$  per complexed ion. The system in study is as follows:  $c_{i,\text{initial}} = 0.605 \text{ mol dm}^{-3}$ ,  $m_{\text{HNO}_3,\text{initial}} = 3 \text{ mol kg}^{-1}$ , and  $m_{\text{Eu}(\text{NO}_3)_3,\text{initial}} = m_{\text{Fe}(\text{NO}_3)_3,\text{initial}} = 0.05 \text{ mol kg}^{-1}$ .

is in agreement with experimental reports and theoretical studies.<sup>11,18,27,33,37,41,47,48</sup> For  $p_0 = 2.5$ , the valley of low  $F_{chain}$  will correspond to high numbers of extractant and water molecules. A similar but less pronounced effect is obtained when  $p_0 = 3$ . Favored aggregation numbers are then 5 and 6, but the water content is still very high. The compositions of such aggregates do not correspond to experimental observations. The equilibrium aggregate probabilities calculated for  $p_0 = 2.5$  and 3 are presented in Figures S3 and S4 in the Supporting Information.

Furthermore, there is another limitation for use of  $p_0$ . For  $p_0 = 2.5$  and 3, the method is not self-consistent. This means that the range of  $N_i$  and  $N_w$  affects the prediction of overall extraction (for all solutes present in the system). The result of the calculation ought to be invariant to the upper limit of  $N_i$

and  $N_w$ . That is another constraint which may as well be a crucial condition when deciding what  $p_0$  value to take for the calculation. The case of  $p_0 = 3.5$  gives a self-consistent calculation, where large  $N_l$  and  $N_w$  do not contribute to the result of the calculation and can, therefore, be neglected.

Another geometrical parameter in our model is the generalized bending constant,  $\kappa^*$ . Therefore, we studied the influence of  $\kappa^*$  on the “valley” of low  $F_{\text{chain}}$  and the equilibrium aggregate probabilities. Previously reported values of adjusted  $\kappa^*$  for reverse aggregates were  $2.5 k_B T$  per DMDOHEMA molecule.<sup>25,26</sup> Recently, a molecular dynamics study done by our group provided a value of  $16 k_B T$  per extractant molecule in heptane solvent.<sup>27</sup> This value points to very high curvature toward water (in the reverse micelles) and was attributed to the strong interactions of  $\text{Eu}^{3+}$  and DMDOHEMA molecules. As a starting point, we used this value for calculations and then changed it by  $\pm 10 k_B T$  per extractant molecule. The results are provided in Figures S5–S7 in the [Supporting Information](#).  $\kappa^*$  influences the width of the chain energy valley in such a way that an increase of  $\kappa^*$  increases the gradient of  $F_{\text{chain}}$  plane. Consequently, higher values of  $\kappa^*$  (in our calculation  $26 k_B T$  per extractant molecule, [Figure S7](#)) allow assembly of aggregates with a smaller number of water molecules. For  $\kappa^* = 6 k_B T$ , the valley of low  $F_{\text{chain}}$  is rather wide, so dilution of the core of the aggregate is highly favorable. As a consequence, aggregates of very different stoichiometry coexist. Most such aggregates are unrealistic compared to the experiments.

It can be concluded that higher rigidity of the extractant film reduces polydispersity in terms of water content. Recall that monodispersity in terms of aggregation number is already achieved through the choice of  $p_0$  and imposed rule  $N_{l,\text{min}} = 4N_{\text{Cat}}$  in the definition of the complexation term.

The choice of  $\kappa^*$  also affects the overall extraction. By varying  $\kappa^*$  from 26 to  $6 k_B T$ , the calculated distribution coefficient varied from 14.6 to 5.6, i.e., nearly a factor of 3. This counterintuitive variation of extraction efficiency with the branching of the chains is always observed in industrial applications but has never been predicted by any model of extraction to the best of our knowledge.<sup>39</sup> The variation of  $\kappa^*$  was also reflected in the CAC value, which was decreased with the decrease of rigidity.

The choice of  $\kappa^* = 16 k_B T$  per extractant molecule is acceptable in both realistic aggregate compositions and the overall extraction prediction.

So far, we have introduced and validated the parameters  $p_0$  and  $\kappa^*$ . In order to calculate the extraction of solutes, we still require standard chemical potential of extractant molecules,  $\mu_1^\circ$ , and complexation energy,  $E_{0,\text{Cat}}$  for the particular solute.

The value of  $\mu_1^\circ$  determines the transition energy between monomeric and aggregated states of the extractant. In our study, the aggregated state has a form of reverse micelles. It is accessible by experimental methods that can determine the mole fraction of the unbound extractant, e.g., NMR shift techniques, scattering extrapolated to zero micelle concentration, or derivatives analysis of liquid–liquid surface tension.<sup>49</sup> In the case of common extractants, the three techniques provided the same result.<sup>50</sup>

Increasing  $\mu_1^\circ$  lowers the transition energy between the two states (eqs 30–34), thus favoring the micellization and the extraction of solutes. A favored micellization is seen as a decrease in CAC and increase in distribution coefficients. A notable property is that the calculated equilibrium aggregate probabilities are invariant to the change of  $\mu_1^\circ$ .  $\mu_1^\circ$  was fitted

accordingly to the experiments, and the value obtained in our study was  $2.5 \text{ kJ/mol}$ .<sup>18</sup>

In order to obtain  $E_{0,\text{Cat}}$  for each solute, namely  $\text{HNO}_3$ ,  $\text{Eu}(\text{NO}_3)_3$ , and  $\text{Fe}(\text{NO}_3)_3$ , we made a fitting based on different known studies. First, we fitted the model to the data concerning the extraction of  $\text{HNO}_3$  alone.<sup>11,42,51,52</sup> This yielded  $E_{0,\text{HNO}_3} = 5 k_B T$ , which is a typical order of magnitude for the hydrogen bond formation. In order to obtain  $E_{0,\text{Eu}(\text{NO}_3)_3}$ , we fitted the experimental data of the  $\text{HNO}_3/\text{Eu}(\text{NO}_3)_3$  system using  $E_{0,\text{HNO}_3}$ .<sup>13</sup> Fitting resulted in  $E_{0,\text{Eu}(\text{NO}_3)_3} = 15.6 k_B T$ . The same procedure was followed for the  $\text{HNO}_3/\text{Fe}(\text{NO}_3)_3$  system, which in turn yielded  $E_{0,\text{Fe}(\text{NO}_3)_3} = 13 k_B T$ .<sup>53</sup> This type of fitting was proposed in order to “isolate” the complexation parameter of each particular cation (i.e., particular solute molecule). By doing this, of course, we neglected any type of interaction between different solutes in the organic phase, and also we forbid the existence of mixed-solute aggregates. Obviously, we made a very crude approximation, but this still makes a good starting point for a study of complex multicomponent systems.  $E_{0,\text{Cat}}$  in our study can be associated with the extraction free energy,  $\Delta G_0$ , from previous studies.  $\Delta G_0$  was defined as the difference between the free energy of an ion in an aqueous phase and that of an ion complexed by extractant molecules in solvent phase.<sup>14</sup> This definition allows a measurement of  $\Delta G_0$  by a combination of calorimetry and EXAFS measurements (coupled with *ab initio* calculations).

In the remainder of this paper, we will show how this model captures a majority of the specific properties of extraction systems.

**Equilibrium Aggregate Probabilities.** With all the parameters determined and discussed, we have performed calculations in an attempt to quantitatively describe a properties of the extraction systems. All the following results are obtained from the calculation with  $p_0 = 3.5$ ,  $\kappa^* = 16 k_B T$  per extractant molecule,  $\mu_1^\circ = 2.5 \text{ kJ/mol}$ ,  $E_{0,\text{HNO}_3} = 5 k_B T$ ,  $E_{0,\text{Fe}(\text{NO}_3)_3} = 13 k_B T$ , and  $E_{0,\text{Eu}(\text{NO}_3)_3} = 15.6 k_B T$ .

The first thing to study is the aggregate compositions. [Figure 3](#) shows calculated equilibrium probabilities of the aggregates for the practical system (the type of the extractant is used in DIAMEX process and aqueous phase represents a system for a REEs recovery via hydrometallurgy) composed of  $m_{\text{HNO}_3,\text{initial}} = 3 \text{ mol kg}^{-1}$ , and  $m_{\text{Eu}(\text{NO}_3)_3,\text{initial}} = m_{\text{Fe}(\text{NO}_3)_3,\text{initial}} = 0.05 \text{ mol kg}^{-1}$  aqueous solution in contact with  $c_{l,\text{initial}} = 0.605 \text{ mol dm}^{-3}$  extractant in heptane solvent. The results are presented for the case where only one salt molecule is inside the core of the aggregates since the calculations showed that addition of second salt molecule pays the huge penalty in terms of chain energy thus making the probabilities negligible. The upper left graph ([Figure 3](#)) shows the probabilities of aggregates filled only with water molecules. Compared to the other types of aggregates, their probability is more than 10 times smaller. This means that in the case of concentrated aqueous solutions in contact with solvent phase, the water extracted to organic phase originates almost entirely from aggregates containing acid or salt molecules. This result is quite understandable since it is known that upon the addition of acid or metal cations to the aqueous phase, the amount of co-extracted water increases.<sup>13,42,52</sup> The upper left and the two bottom graphs (also [Figure 3](#)) show the probabilities for aggregates

containing, in the same order,  $\text{Eu}(\text{NO}_3)_3$ ,  $\text{HNO}_3$ , and  $\text{Fe}(\text{NO}_3)_3$  molecules. In contrast to the case when only water molecules are present inside the core, the highest probabilities in terms of  $N_w$  are at compositions from 4 to 5 water molecules per aggregate for  $\text{HNO}_3$ , whereas from 6 to 8 water molecules for  $\text{Eu}(\text{NO}_3)_3$  and  $\text{Fe}(\text{NO}_3)_3$  molecules. This is a consequence of the differences in chemical potentials of ions and water between the aqueous and the organic (solvent) phases. The higher water content for  $\text{Eu}(\text{NO}_3)_3$  and  $\text{Fe}(\text{NO}_3)_3$  salts is due to the higher number of particles in the core of the aggregate. The dilution of the core is a highly favorable effect that stabilizes the aggregates core, but it works in opposite way with respect to the  $F_{\text{chain}}$  because the inclusion of additional particles causes the increase in core radius (an unfavorable swelling of the reverse micelle). Another important thing to add here is that the probability of particular aggregate is not only governed by the dominant term  $E_{0,\text{Cat}}$  but also depends on the composition of the entire system in study, i.e., on the initial extractant, acid and ion concentrations, temperature, etc. For example, if there is a change of reservoir acid or metal cation concentrations, the distribution of aggregates, i.e., the probabilities at equilibrium, will be different. To emphasize this, we performed the calculations for different concentrations of acid and lanthanides. The results are presented in Figures S8 and S9 in the Supporting Information. This important property is also reflected in the aggregation threshold, the apparent stoichiometry, and the overall extraction efficiency, as we will show in the following part of the discussion. We emphasize again that all subsequent calculations were done with values of parameters  $p_0 = 3.5$ ,  $\kappa^* = 16 k_B T$  per extractant molecule,  $\mu_1^\circ = 2.5 \text{ kJ/mol}$ ,  $E_{0,\text{HNO}_3} = 5 k_B T$ ,  $E_{0,\text{Fe}(\text{NO}_3)_3} = 13 k_B T$ , and  $E_{0,\text{Eu}(\text{NO}_3)_3} k_B T = 15.6 k_B T$  per complexed ion.

**Predicting the Aggregation Threshold, i.e., the Critical Aggregate Concentration.** We have already stated that one of the crucial properties of extraction system is measured CAC. We tried to mimic different systems, which are often found in the literature and to calculate corresponding CAC. Figure 4 shows the calculated equilibrium concentrations of both monomeric and aggregated extractant molecules as a function of initial (or total) extractant concentration. Figure 4a shows the concentrations of the extractant for  $\text{LiNO}_3$  aqueous solution in contact with a

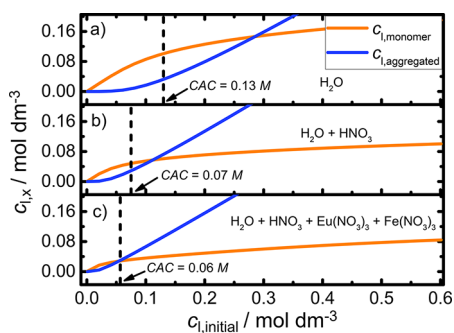


**Figure 4.** Calculated concentrations of monomeric and aggregated extractant as a function of the initial (or total) extractant concentration. Solvent phase in contact to (a)  $m_{\text{LiNO}_3,\text{initial}} = 3 \text{ mol kg}^{-1}$  (nonextracted salt), (b)  $m_{\text{HNO}_3,\text{initial}} = 3 \text{ mol kg}^{-1}$ , and (c)  $m_{\text{HNO}_3,\text{initial}} = 3 \text{ mol kg}^{-1}$  and  $m_{\text{Eu}(\text{NO}_3)_3,\text{initial}} = m_{\text{Fe}(\text{NO}_3)_3,\text{initial}} = 0.05 \text{ mol kg}^{-1}$ . The black dashed line shows the calculated critical aggregate concentration.

solvent, which represents a typical background non-extracted salt system. As shown in the figure, CAC for such a system is evaluated to be  $0.13 \text{ mol dm}^{-3}$  initial extractant concentration, and only water molecules are present in the aggregates. Figures 4b–c show respectively the system of a  $\text{HNO}_3$  aqueous solution and a mixture of  $\text{HNO}_3$ ,  $\text{Eu}(\text{NO}_3)_3$ , and  $\text{Fe}(\text{NO}_3)_3$  in contact with the solvent phase. The details of the concentrations in each system are given in the caption of Figure 4. Upon the addition of acid and cations in the system, CAC decreased to 0.07 and 0.06 M, respectively.

Figure 5 demonstrates that the model captures a known decrease of CAC upon the addition of acid in the system. The

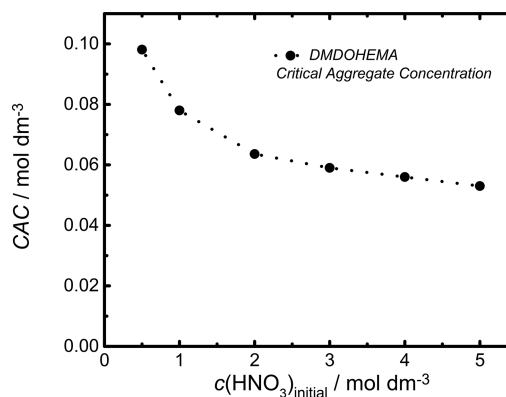


**Figure 5.** Critical aggregate concentration as a function of  $\text{HNO}_3$  concentration. The system in study is  $c_{l,\text{initial}} = 0.6 \text{ mol dm}^{-3}$ ,  $m_{\text{Eu}(\text{NO}_3)_3,\text{initial}} = m_{\text{Fe}(\text{NO}_3)_3,\text{initial}} = 0.05 \text{ mol kg}^{-1}$ .

results of the CAC as a function of initial  $\text{HNO}_3$  concentration in aqueous phase presented here are made for the system  $c_{l,\text{initial}} = 0.6 \text{ mol dm}^{-3}$ ,  $m_{\text{Eu}(\text{NO}_3)_3,\text{initial}} = m_{\text{Fe}(\text{NO}_3)_3,\text{initial}} = 0.05 \text{ mol kg}^{-1}$ . The enhancement of the micellization is due to the two factors contributing to the free energy of the aggregates. The first and more dominant factor is the increase of the solute concentration able to make a weak complex with the extractant molecule (defined by complexation energy  $E_{0,\text{HNO}_3}$ ). The second factor is an increase of  $\text{NO}_3^-$  concentrations ratio between the aqueous phase and the core of the aggregate (eq 34). The properties of the extracting systems shown in Figures 4 and 5 correspond to experimental findings.<sup>48,51</sup>

**Prediction of the Extraction Process.** It is often convenient to show the evolution of solute concentrations in the organic phase as a function of  $c_{l,\text{initial}}$ . Therefore, in Figure 6 we show the extraction curves of all species for a system  $m_{\text{HNO}_3,\text{initial}} = 3 \text{ mol kg}^{-1}$ ,  $m_{\text{Eu}(\text{NO}_3)_3,\text{initial}} = m_{\text{Fe}(\text{NO}_3)_3,\text{initial}} = 0.05 \text{ mol kg}^{-1}$ . An important feature is the low extraction of  $\text{HNO}_3$  compared to the literature. This is a consequence of our approximation that only one type, acid or metal nitrate molecule, can occupy the aggregate. In future publications, the complexation term will be defined in a more realistic way, which will result in a proper  $\text{HNO}_3$  extraction curve. Still, different trends can be observed while inspecting Figure 6. A typical high water uptake and an increased metal nitrate extraction with an increase in  $c_{l,\text{initial}}$  correlate extremely well with the experiments.<sup>42</sup> Also, it is worth to mention that before CAC the aggregation is controlled by water extraction because of a smaller penalty in chain energy while after CAC, the aggregation is entirely controlled by complexation of metal nitrates. The results showing the concentrations of the

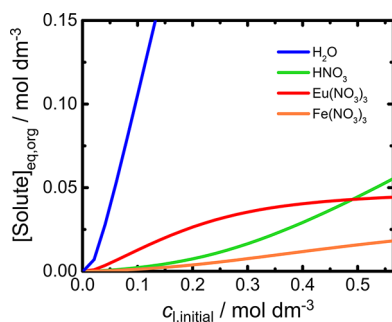


**Figure 6.** Calculated equilibrium concentrations of all extracted solutes as a function of the initial extractant concentration. The system in study is  $m_{\text{HNO}_3, \text{initial}} = 3 \text{ mol kg}^{-1}$ ,  $m_{\text{Eu}(\text{NO}_3)_3, \text{initial}} = m_{\text{Fe}(\text{NO}_3)_3, \text{initial}} = 0.05 \text{ mol kg}^{-1}$ .

extracted solutes as a function of the initial extractant concentration for different acidity and initial salt concentrations are presented in Figure S10 in the [Supporting Information](#). The results show that extraction efficiency is strongly dependent on the composition of the system, i.e., on the initial acid and salt concentrations.

The concentration of acid in the aqueous phase influences the extraction of cations.<sup>42</sup> In order to test our model we made a set of calculations for different  $\text{HNO}_3$  aqueous concentrations. The extraction efficiency is usually expressed as

$$D_{\text{Cat},i} = \frac{\sum_{\text{wil}} c_{A_{N_w, N_i, N_l}} N_{\text{Cat},i}}{m_{\text{eq},i}^{\text{aq}}} = \frac{c_{\text{Cat},i}^{\text{org}}}{m_{\text{eq},i}^{\text{aq}}} \quad (38)$$

where  $D_{\text{Cat},i}$  is a distribution coefficient of target solute between aqueous and solvent phases at equilibrium and  $c_{\text{Cat},i}^{\text{org}}$  is the total concentration of solute in the organic phase.<sup>54</sup> If one wants to express  $D_{\text{Cat},i}$  as a fraction of molar concentrations, a usual conversion of molality in aqueous phase is made with relation  $c_i^{\text{aq}} = \rho^{\text{aq}} m_i^{\text{aq}} / (1 + \sum_i m_i^{\text{aq}} M_i)$ , where  $\rho^{\text{aq}}$  is the density of the aqueous solution.

$D_{\text{Eu}^{3+}}$  and  $D_{\text{Fe}^{3+}}$  as a function of  $c_{i, \text{initial}}$  have been calculated for different  $m_{\text{HNO}_3, \text{initial}}$  (different acidity of aqueous phase) and presented in Figure S8 in the [Supporting Information](#). The results show the nonlinear increase of distribution coefficients with increasing  $c_{i, \text{initial}}$ . The increase in  $m_{\text{HNO}_3, \text{initial}}$  causes an increase in  $D_{\text{Cat},i}$  which means that the extraction is enhanced upon addition of  $\text{HNO}_3$  the system. This is again the consequence of an increase of  $\text{NO}_3^-$  concentrations ratio between the aqueous phase and the core of the aggregate.

Another way of plotting these results is by employing so-called “log–log” plot, as it is traditionally made in the slope method to investigate the apparent stoichiometry of the system.<sup>55,56</sup> In this manner we have transformed the data from [Figure S8](#) to decimal logarithms and presented them in [Figure 7](#). [Figure 7a](#) shows again the extraction for different  $\text{HNO}_3$  concentrations. It can be noticed that depending on the region of  $c_{i, \text{initial}}$  the slope of the extraction lines changes and typically three regimes are observed. Moreover, the trend in change of slope is dependent on the acidity of system, i.e., on  $\text{HNO}_3$  concentrations. Below typically  $m_{\text{HNO}_3, \text{initial}} = 2 \text{ mol kg}^{-1}$  the calculations have shown a different behavior than for higher concentrations. In order to see the differences better, we have isolated the graphs for  $m_{\text{HNO}_3, \text{initial}} = 0.5$  (black line) and  $5 \text{ mol kg}^{-1}$  (red line) and plotted them separately in [Figure 7b](#). What is striking is the fact that slope changes substantially for

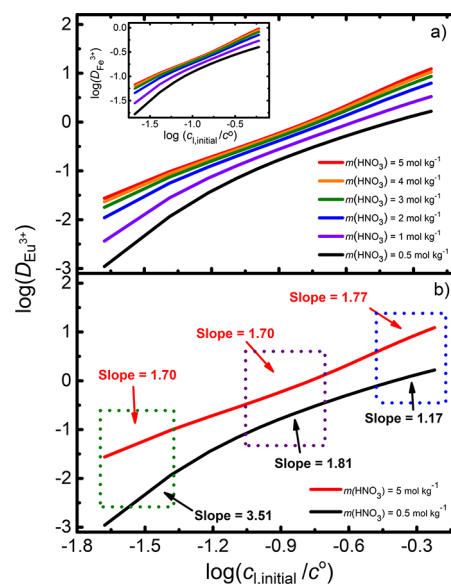


**Figure 7.** (a) Decimal logarithm of  $\text{Eu}^{3+}$  distribution coefficient as a function of decimal logarithm of the initial extractant concentration. The system in study is  $c_{i, \text{initial}} = 0.6 \text{ mol dm}^{-3}$ ,  $m_{\text{Eu}(\text{NO}_3)_3, \text{initial}} = m_{\text{Fe}(\text{NO}_3)_3, \text{initial}} = 0.05 \text{ mol kg}^{-1}$ . The results are presented for various concentrations of nitric acid in aqueous phase. The equivalent curve for the extraction of  $\text{Fe}^{3+}$  is presented in the inset. (b) Slope method results for  $m_{\text{HNO}_3, \text{initial}} = 0.5$  and  $5 \text{ mol dm}^{-3}$ .

$m_{\text{HNO}_3, \text{initial}} = 0.5 \text{ mol kg}^{-1}$ , depending on  $c_{i, \text{initial}}$ . A high initial slope of approximately 3.5 is followed by 1.8 and then 1.2. The case of  $m_{\text{HNO}_3, \text{initial}} = 5 \text{ mol kg}^{-1}$  shows again the three regimes but in all regions slope is around 1.7. This observation points to the fact that high salt concentrations in aqueous phase tend to damp the fine-tuning influences on the apparent extraction stoichiometry. In practice, by considering a large concentration range the log–log plots are usually not straight lines. There is a deviation at both low and high extractant concentrations. When the central slope is used, the non-integer value is said to correspond to the average effective stoichiometry. If the slope at a given range of concentrations is not an integer, several different complexes are invoked. Furthermore, the complexation at low extractant concentration is higher. Obtaining a larger aggregation number is contrary to the Le Chatelier’s principle. This difficulty has been discussed in chemical engineering for different types of adducts, i.e., molecules which participate in the aggregate but are not complexed. All the extra parametrization which is necessary when the slope method is applied is no longer required using our general model. Without any extra parameters, the extraction and its intrinsic non-linearity are predicted.<sup>57,58</sup> This finding brings attention to the longstanding use of the slope method in determination of the stoichiometry for various hydrometallurgical processes. We wish to emphasize that, under a certain physical condition of the system, various regimes in stoichiometry can be “masked” by experimental error, thus leading to false simplicity in the understanding of the behavior of the system.<sup>59</sup> Besides the concentration of nitric acid, we have varied the concentrations of the lanthanide. As expected, the apparent stoichiometry is dependent on the initial concentration of target solutes. The results are presented in the [Supporting Information](#).

Figure 8 shows the dependence of  $D_{\text{Eu}^{3+}}$  from the mixture of salts on the  $\text{HNO}_3$  concentrations. This represents a part of

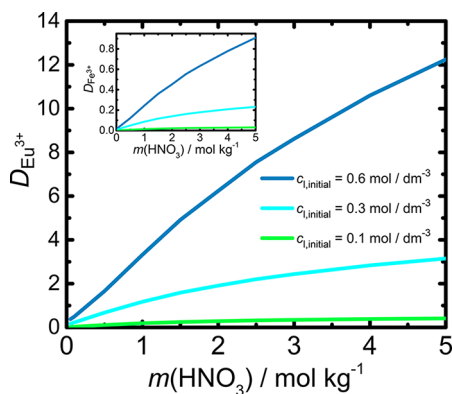


**Figure 8.**  $\text{Eu}^{3+}$  distribution coefficient as a function of nitric acid concentration in aqueous phase. The system in study is  $c_{i,\text{initial}} = 0.6 \text{ mol dm}^{-3}$ ,  $m_{\text{Eu}(\text{NO}_3)_3,\text{initial}} = m_{\text{Fe}(\text{NO}_3)_3,\text{initial}} = 0.05 \text{ mol kg}^{-1}$ .

the multicomponent phase diagram along the fraction of acid in the aqueous phase. Calculations are done for the extractant concentrations after the CAC, which ensures that we are in the regime where the aggregates are the dominant species in the solvent. The results show that, in fact, our model recovers typical Langmuir isotherms that have already been reported by both experiment and modeling.<sup>13,51</sup> For  $0.1 \text{ mol dm}^{-3}$ , the extractant is entirely saturated and an additional increase of  $\text{HNO}_3$  concentration cannot enhance the extraction. In contrast, when the concentration of the extractant is  $0.6 \text{ mol dm}^{-3}$ , there is a sufficient amount of monomers. Adding  $\text{HNO}_3$  in the aqueous phase pushes the equilibrium toward the creation of the additional aggregates containing  $\text{Eu}^{3+}$ .

**Complexation Energy Study and Reversible Formulations.** In hydrometallurgy, the extraction of a cation to the solvent phase is often identified as the complexation of a cation by the chelating agent (the extractant molecule). In fact, the affinity to form the complex is indeed the leading force for extraction of the cation, but it is only one of the terms in the global free energy of transfer.<sup>14</sup> In our model, complexation is counterbalanced by a few opposing forces such as energy cost for packing of extractant chains in ordered film, i.e., a steric hindrance, the differences in ion concentrations between the aqueous and the solvent phases, the differences in chemical potentials of water between two phases, etc. (see full expression for free energy of aggregate in Appendix A).

In order to clarify this misunderstanding, we plotted the negative value of the natural logarithm of the  $D_{\text{Eu}^{3+}}$  as a function of the negative value of the complexation parameter  $E_{0,\text{Eu}(\text{NO}_3)_3}$ . By declaring  $E_{0,\text{Eu}(\text{NO}_3)_3}$  as a continuous variable, we mimic the strength (or affinity) of the extractant molecule to form a complex with  $\text{Eu}^{3+}$ . Different types of extractants are characterized by a different  $E_{0,\text{Eu}(\text{NO}_3)_3}$ .

The term  $-k_B T \ln D_{\text{Eu}^{3+}}$  is often referred to as the apparent energy of the extraction.<sup>26</sup> In Figure 9, the assumption complexation = extraction (a green dashed line) is plotted for purpose of easier understanding of the context. Figures 9a–b show the  $-k_B T \ln D_{\text{Eu}^{3+}}/k_B T$  for a system  $c_{\text{Eu}(\text{NO}_3)_3,\text{initial}} = 0.1 \text{ mol dm}^{-3}$  and  $c_{\text{Eu}(\text{NO}_3)_3,\text{initial}} = 1 \text{ mol dm}^{-3}$ , respectively. The extractant concentration was fixed to  $c_{i,\text{initial}} = 0.6 \text{ mol dm}^{-3}$ . The two different initial  $\text{Eu}^{3+}$  concentrations represent the

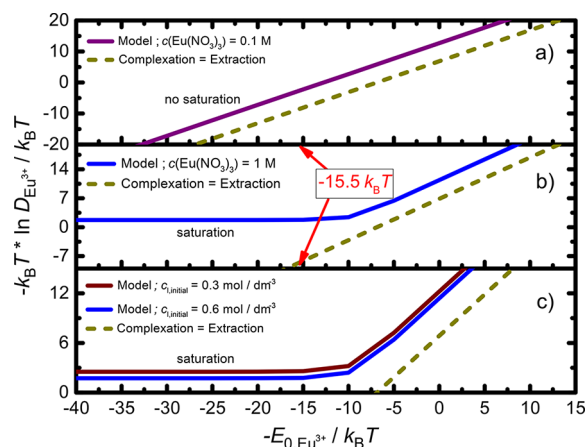


**Figure 9.** Negative value of natural logarithm of the distribution coefficient  $-\ln D_{\text{Eu}^{3+}}$  as a function of a negative value of the complexation energy parameter  $E_{0,\text{Eu}(\text{NO}_3)_3}$ . The negative values of  $E_{0,\text{Eu}(\text{NO}_3)_3}$  are taken for the purpose of visually easier reading of the saturation limit. (a) System:  $c_{i,\text{initial}} = 0.6 \text{ mol dm}^{-3}$ ,  $c_{\text{Eu}(\text{NO}_3)_3,\text{initial}} = 0.1 \text{ mol dm}^{-3}$ . (b) System:  $c_{i,\text{initial}} = 0.6 \text{ mol dm}^{-3}$ ,  $c_{\text{Eu}(\text{NO}_3)_3,\text{initial}} = 1 \text{ mol dm}^{-3}$ . (c) System:  $c_{\text{Eu}(\text{NO}_3)_3,\text{initial}} = 1 \text{ mol dm}^{-3}$ . The calculations are shown for the two initial extractant concentrations, namely  $c_{i,\text{initial}} = 0.6 \text{ mol dm}^{-3}$  and  $c_{i,\text{initial}} = 0.3 \text{ mol dm}^{-3}$ .

cases below and above the experimentally observed limiting organic concentration (LOC) of solutes. This view is quite useful when developing an efficient formulation for the extraction.

Two immediate conclusions can be drawn. First, the extraction cannot be solely identified with the complexation energy, since solid and dashed lines are not collinear. Second, the choice of the extractant is also dependent on the concentration of the target metal cation and not only on its nature. When a concentration of metal cation is sufficiently low compared to the concentration of the extractant (Figure 9a), the  $E_{0,\text{Eu}(\text{NO}_3)_3}$  can be very high (typically that of the ionic charged extractant) and saturation would still not occur. By saturation, in this context, we address the case where most of the extractant molecules are in aggregated form and the concentration of monomeric form is almost negligible. In Figure 9b for  $c_{\text{Eu}(\text{NO}_3)_3,\text{initial}} = 1 \text{ mol dm}^{-3}$ , the saturation is achieved already for the type of extractant described by typically  $E_{0,\text{Eu}(\text{NO}_3)_3} = 10 k_B T$  per complexed ion, thus showing an irreversible character of the formulation. This means that, in practical formulation, it would be sufficient to use a lower concentration of salt or to exchange DMDOHEMA extractant with some less efficient one.

An important feature of this model is the use of well-defined and justified parameters. The results presented in Figure 9 provide a sort of justification of  $E_{0,\text{Cat}}$  in general.  $E_{0,\text{Cat}}$  has a proper value if and only if, for a given definition (recall Theory section, eq 14), it provides a result which is in accordance with the experimental values. A value of  $E_{0,\text{Eu}(\text{NO}_3)_3} = 15.6 k_B T$  is in fact a good value for the description since it corresponds to approximately  $D_{\text{Eu}^{3+}} = 11$  (Figure 9a). A conclusion is that the system composed of  $c_{\text{Eu}(\text{NO}_3)_3,\text{initial}} = 0.1 \text{ mol dm}^{-3}$  in 3 M nitric acid and DMDOHEMA extractant in a solvent represents a desirable reversible formulation.

Figure 9c shows the influence of total extractant concentration,  $c_{i,\text{initial}} = 0.3$  and  $0.6 \text{ mol dm}^{-3}$ . The important feature is that saturation is achieved for the same  $E_{0,\text{Eu}(\text{NO}_3)_3}$  value. The only difference is between the two is that formulation with the higher  $c_{i,\text{initial}}$  can extract more of the target ion.

In hydrometallurgy, the supramolecular approach stipulates that the extraction free energy corresponds to the complexation of the cation by one or more chelating agents (synonym for the extractant molecules) associated with an entropy of mixing.<sup>9</sup> In the colloidal approach proposed here, a more general view is now possible. That is why we propose Figure 9 to illustrate this.<sup>14</sup> Since the negative value of the natural logarithm of  $D_{\text{Eu}^{3+}}$  represents the apparent free energy of the electrolyte extraction, we plot this quantity related to the efficiency on  $y$ -axis, while  $x$ -axis shows the chemical motor driving the transfer toward the phase containing the extractant. The latter is specific to each lanthanide/extractant couple. Figure 9a shows the case where the mole ratio of the extractant to lanthanide is a factor of 6, and we see that in these conditions, the usual supramolecular approximation holds. The two lines are separated by around  $7 k_B T$ , which corresponds to the sum of various contributions included within our model, namely, differences in ion concentrations between the core of the aggregate and the aqueous phase, the differences in chemical potentials of water between two phases, steric hindrance of extractant chains, etc. The opposite case is shown in Figure 9b, where now the amount of lanthanide cations is in excess relative to the amount of extractant molecules in the system. In this case, the curves exhibit the typical Langmuir isotherm's behavior since, after the saturation of the extractants, the extraction efficiency no longer depends on the driving complexation energy. We show an order of magnitude for our practical case of DMDOHEMA/ $\text{Eu}^{3+}$  to which the complexation parameter has been attributed (via fitting procedure). Last but not the least, in this case, monomer concentrations are negligible, and this favors the danger of going in the three-phase triangles since the oil phase becomes unstable.<sup>12</sup>

## CONCLUSION

In order to acquire insight into the forces that influence the aggregation process and to predict the overall extraction of solutes into a solvent phase, we proposed a minimal model for which the parameters are experimentally accessible. The minimal model was derived from statistical thermodynamics within a framework of molecular self-assembly of the extractant molecules. With this colloidal approach that goes beyond supramolecular chemistry considerations, the efficiency plots can be generated for any point of a Winsor II regime where the dominant aggregates are reverse spherical micelles.

Our model, in a global free energy difference approach, takes into account the dominant term called complexation free energy, which is well known in organometallic chemistry of supramolecular self-assembly. The complexation free energy is counterbalanced by weaker quenching terms associated with the packing of extractant chains, differences in ion concentrations between the two phases, water activity, etc. To the best of our knowledge, the model presented here uses quantitatively, for the first time, both generalized bending constant  $\kappa^*$  and spontaneous packing parameter  $p_0$  larger than 2 for evaluating phase transfers.

The free energy associated with the film of extractant chains,  $F_{\text{chain}}$ , is a function of parameter  $p_0$ . By adjusting  $p_0$ , we showed that positioning of the valley of low  $F_{\text{chain}}$  greatly influences the composition of the aggregates at thermodynamic equilibrium. Realistic compositions were obtained for  $p_0 = 3.5$ . Lower  $p_0$  favors unrealistically high aggregation numbers and water contents in the core of the aggregates.

Rigidity  $\kappa^*$  adjusts the number of water molecules inside the core of the aggregate. A decrease in  $\kappa^*$  increases polydispersity and causes an unrealistically high water uptake. A higher  $\kappa^*$  decreases the number of water molecules inside the core, thus providing more realistic aggregate compositions, but it also quenches the extraction (and increases CAC). The value we have validated with our calculations is  $\kappa^* = 16 k_B T$  per extractant molecule.

Fitting of experimental CAC and extraction curves yielded the standard chemical potential  $\mu_1^\circ = 2.5 \text{ kJ/mol}$ , and the complexation energies, namely,  $E_{0,\text{HNO}_3} = 5 k_B T$ ,  $E_{0,\text{Fe}(\text{NO}_3)_3} = 13 k_B T$ , and  $E_{0,\text{Eu}(\text{NO}_3)_3} = 15.6 k_B T$ .

With the obtained parameters, we studied a practical system composed of  $\text{HNO}_3$ ,  $\text{Eu}(\text{NO}_3)_3$ , and  $\text{Fe}(\text{NO}_3)_3$  aqueous solution in contact with a solvent containing DMDOHEMA extractant. The calculations showed that the most probable aggregates contain typically one salt molecule, four extractants, and from 4 to 8 water molecules inside the core (depending on the type of salt). Stable aggregates containing  $\text{Eu}(\text{NO}_3)_3$  or  $\text{Fe}(\text{NO}_3)_3$  are formed with an increased number of water molecules, since more ions in the core require a higher dilution in order to reach a stable form. The probabilities, and thus the concentrations, of the aggregates at equilibrium are dependent not only on the interaction of extractant and extracted solutes (i.e., on  $E_{0,\text{Cat}}$ ) but also on the composition of the entire system, e.g., the initial acid and salt concentrations, temperature, etc.

Our model predicts a decrease of CAC upon the addition of target salts in the aqueous phase. An increase of  $\text{HNO}_3$  concentration forces higher water co-extraction and also enhances the extraction of metal nitrates, namely  $\text{Eu}(\text{NO}_3)_3$  and  $\text{Fe}(\text{NO}_3)_3$ .

The extractant concentration, especially above CAC for a particular system, plays a significant role in the extraction of target salts. The calculated distribution coefficient versus extractant concentration results shows nonlinear behavior, which is even more pronounced upon increasing the bulk  $\text{HNO}_3$  concentration. A slope method used to determine the apparent stoichiometry of complexation shows different trends that depend not only on extractant but also on the acid and lanthanide concentrations.

In the context of reversible and therefore desirable formulations for the extraction systems, we have performed calculations with varying  $E_{0,\text{Eu}(\text{NO}_3)_3}$ . The results show that choice of extractant is dependent on, besides the nature of the target salt, also its total concentration in the aqueous phase. The calculations show that there is a threshold of  $E_{0,\text{Eu}(\text{NO}_3)_3}$  after which the saturation of extractant is achieved (for a defined salt concentration), thus making an unfavorable formulation. Upon increasing the total extractant concentration, as expected, the extraction capacity of the used formulation increases, but the saturation threshold remains constant. Therefore, saturation in terms of  $E_{0,\text{Eu}(\text{NO}_3)_3}$  is not a function of the total extractant concentration,  $c_{i,\text{initial}}$ .

Our calculations also show a clear distinction between extraction of the solute and the complexation energy term.

In our next publication, extension to charged extractants will be considered. This implies ion exchange between oil and water phases, instead of extraction of a neutral salt molecule.<sup>60</sup> Such extension greatly broadens the applicability of the model to many commonly used industrial systems.<sup>2</sup>

## ■ APPENDIX A

A full expression for the free energy of aggregates core (with at least one salt molecule inside) reads

$$\begin{aligned}
 F_{\text{core}} = & \\
 & -k_{\text{B}}T \ln N_{\text{complex}} - N_{\text{Cat}}E_{0,\text{Cat}} + k_{\text{B}}T \ln \left( N_{\text{w}}! \prod_i N_i! \right) \\
 & - k_{\text{B}}T \left( N_{\text{w}} \ln N_{\text{w}} + \sum_i N_i \ln N_i - N_{\text{w}} - \sum_i N_i \right) \\
 & + N_{\text{w}}\mu_{\text{w}}^{\circ} - k_{\text{B}}TN_{\text{w}} \frac{\sum_i x_i^{\text{org}}}{x_{\text{w}}^{\text{org}}} + \sum_i N_i\mu_i^{\circ} \\
 & + k_{\text{B}}T \sum_i N_i \ln \left( \frac{m_i^{\text{org}}}{m_i^{\circ}} \right) \quad (39)
 \end{aligned}$$

At this point we can also add the chain term  $F_{\text{chain}}$  to recover the full expression for the free energy of the aggregate of particular composition. We have

$$\begin{aligned}
 \mu_{\text{Agg}_{N_{\text{w}},N_i,N_1}}^{\circ} = F_{\text{Agg}_{N_{\text{w}},N_i,N_1}} = & \\
 & -k_{\text{B}}T \ln N_{\text{complex}} - N_{\text{Cat}}E_{0,\text{Cat}} + k_{\text{B}}T \ln \left( N_{\text{w}}! \prod_i N_i! \right) \\
 & - k_{\text{B}}T \left( N_{\text{w}} \ln N_{\text{w}} + \sum_i N_i \ln N_i - N_{\text{w}} - \sum_i N_i \right) \\
 & + N_{\text{w}}\mu_{\text{w}}^{\circ} - k_{\text{B}}TN_{\text{w}} \frac{\sum_i x_i^{\text{org}}}{x_{\text{w}}^{\text{org}}} + \sum_i N_i\mu_i^{\circ} \\
 & + k_{\text{B}}T \sum_i N_i \ln \left( \frac{m_i^{\text{org}}}{m_i^{\circ}} \right) + \frac{N_1}{2} \kappa^* \\
 & \left( 1 + \frac{l_{\text{chain}}}{R_{\text{core}}} + \frac{1}{3} \frac{l_{\text{chain}}^2}{R_{\text{core}}^2} - p_0 \right)^2 \quad (40)
 \end{aligned}$$

with  $R_{\text{core}}$  being already calculated through the following relation:

$$R_{\text{core}} = \sqrt[3]{\frac{3}{4\pi} \left( \sum_i N_i V_{\text{m},i} + N_{\text{w}} V_{\text{m},\text{w}} + N_1 V_{\text{m},1} \right)}$$

## ■ APPENDIX B

### Algorithm for Finding a Numerical Solution of Multicomponent Systems

The calculation were preformed in a semi-grand canonical ensemble (we only considered a reservoir of water molecules).<sup>30</sup> Therefore, in order to obtain a correct equilibrium concentrations of the extractant and aggregates in solvent and ions in aqueous phase, we need to minimize the

law of mass action for any specie simultaneously. Since eq 33 is a monotonic increasing function, the root of it was found using the bisection method.<sup>61</sup> The algorithm for finding the solution for the described system of equations was based on the self-consistent approach. The each specie in the system represents additional dimension for the minimisation. The algorithm to calculate the equilibrium concentrations of all species is as follows:

1. Calculate equilibrium aggregate concentrations using initial concentrations of species which are provided as an input.
2. Find the root of eq 33 using the bisection method.
3. Calculate equilibrium aggregate concentrations again using newly calculated equilibrium extractant concentrations (the root of eq 33).
4. Use bisection method to find equilibrium concentrations of each ionic specie present in the system.
5. Repeat the procedure until the two consecutive calculations do not provide different values (up to convergence limit).
6. Calculate thermodynamic properties of the system.

To reduce a numerical noise, the minimization cycles were ordered in a such a way that extractant and the species with the lowest value of concentrations (such as  $\text{Eu}^{3+}$  or  $\text{Fe}^{3+}$ ) were calculated until the relative difference of calculated equilibrium concentrations between two subsequent calculations was less than  $1 \times 10^{-8}$ . For the species with higher concentrations (such as  $\text{NO}_3^-$ ) the relative difference was set to  $1 \times 10^{-5}$ .

CAC represents the intersection of two linear functions, which are fits of calculated equilibrium monomeric extractant concentrations. The first fit provides the slope of monomeric extractant concentration before CAC, whereas the second fit provides the slope sufficiently after the CAC.

## ■ ASSOCIATED CONTENT

### Supporting Information

The Supporting Information is available free of charge on the ACS Publications website at DOI: 10.1021/acs.langmuir.8b01759.

Study of aggregate probabilities and extraction of metal ions at various physical conditions, including Figures S1–S12 (PDF)

## ■ AUTHOR INFORMATION

### Corresponding Authors

\*E-mail: [mario.spadina@gmail.com](mailto:mario.spadina@gmail.com).

\*E-mail: [jean-francois.dufreche@icsm.fr](mailto:jean-francois.dufreche@icsm.fr).

### ORCID

Mario Špadina: 0000-0002-8292-5765

Klemen Bohinc: 0000-0003-2126-8762

### Notes

The authors declare no competing financial interest.

## ■ ACKNOWLEDGMENTS

The research leading to these results has received funding from the European Research Council under the European Union's Seventh Framework Programme (FP/2007-2013)/ERC Grant Agreement no. 320915, "REE-CYCLE": Rare Earth Element reCYCling with Low harmful Emissions. Research Agency for support through grant BIFR/CEA/16-18-002 and the Slovenian Research Agency for support through program P3-

0388 are acknowledged. The authors would like to thank Magali Duvail, Maximilian Pleines, Barbara Kuzmić, and Simon Gourdin for useful discussions.

## REFERENCES

- (1) Jha, M. K.; Kumari, A.; Panda, R.; Rajesh Kumar, J.; Yoo, K.; Lee, J. Y. Review on hydrometallurgical recovery of rare earth metals. *Hydrometallurgy* **2016**, *165*, 2–26.
- (2) Yoon, H. S.; Kim, C. J.; Chung, K. W.; Kim, S. D.; Lee, J. Y.; Kumar, J. R. Solvent extraction, separation and recovery of dysprosium (Dy) and neodymium (Nd) from aqueous solutions: Waste recycling strategies for permanent magnet processing. *Hydrometallurgy* **2016**, *165*, 27–43.
- (3) Du, X.; Graedel, T. E. Global rare earth in-use stocks in NdFeB permanent magnets. *J. Ind. Ecol.* **2011**, *15*, 836–843.
- (4) Binneemans, K.; Jones, P. T.; Blanpain, B.; Van Gerven, T.; Yang, Y.; Walton, A.; Buchert, M. Recycling of rare earths: A critical review. *J. Cleaner Prod.* **2013**, *51*, 1–22.
- (5) Xie, F.; Zhang, T. A.; Dreisinger, D.; Doyle, F. A critical review on solvent extraction of rare earths from aqueous solutions. *Miner. Eng.* **2014**, *56*, 10–28.
- (6) Walters, A.; Lusty, P.; Hill, A. *Rare earth elements*, Commodity Profiles Series; British Geological Survey, 2011.
- (7) Madic, C.; Lecomte, M.; Baron, P.; Boullis, B. Separation of long-lived radionuclides from high active nuclear waste. *C. R. Phys.* **2002**, *3*, 797–811.
- (8) Modolo, G.; Vijgen, H.; Serrano-Purroy, D.; Christiansen, B.; Malmbeck, R.; Sorel, C.; Baron, P. DIAMEX counter-current extraction process for recovery of trivalent actinides from simulated high active concentrate. *Sep. Sci. Technol.* **2007**, *42*, 439–452.
- (9) Wilson, A. M.; Bailey, P. J.; Tasker, P. A.; Turkington, J. R.; Grant, R. A.; Love, J. B. Solvent extraction: the coordination chemistry behind extractive metallurgy. *Chem. Soc. Rev.* **2014**, *43*, 123–134.
- (10) Testard, F.; Berthon, L.; Zemb, T. Liquid-liquid extraction: An adsorption isotherm at divided interface? *C. R. Chim.* **2007**, *10*, 1034–1041.
- (11) Déjugnat, C.; Berthon, L.; Dubois, V.; Meridiano, Y.; Dourdain, S.; Guillaumont, D.; Pellet-Rostaing, S.; Zemb, T. Liquid-Liquid Extraction of Acids and Water by a Malonamide: I-Anion Specific Effects on the Polar Core Microstructure of the Aggregated Malonamide. *Solvent Extr. Ion Exch.* **2014**, *32*, 601–619.
- (12) Erlinger, C.; Belloni, L.; Zemb, T.; Madic, C. Attractive interactions between reverse aggregates and phase separation in concentrated malonamide extractant solutions. *Langmuir* **1999**, *15*, 2290–2300.
- (13) Muller, J. Spéciation dans les phases organiques des systèmes d'extraction liquide-liquide contenant un malonamide et un acide alkylphosphorique. Ph.D. Thesis, Rapport CEA-R-6159, Université Pierre et Marie Curie, 2012.
- (14) Duffrêche, J.-F.; Zemb, T. Effect of long-range interactions on ion equilibria in liquid-liquid extraction. *Chem. Phys. Lett.* **2015**, *622*, 45–49.
- (15) Zemb, T.; Bauer, C.; Bauduin, P.; Belloni, L.; Déjugnat, C.; Diat, O.; Dubois, V.; Duffrêche, J.-F.; Dourdain, S.; Duvail, M.; Larpent, C.; Testard, F.; Pellet-Rostaing, S. Recycling metals by controlled transfer of ionic species between complex fluids: en route to "ienais. *Colloid Polym. Sci.* **2015**, *293*, 1–22.
- (16) Beltrami, D.; Chagnes, A.; Haddad, M.; Laureano, H.; Mokhtari, H.; Courtaud, B.; Jugé, S.; Cote, G. Solvent extraction studies of uranium(VI) from phosphoric acid: Role of synergistic reagents in mixture with bis(2-ethylhexyl) phosphoric acid. *Hydrometallurgy* **2014**, *144–145*, 207–214.
- (17) Dartiguelongue, A.; Chagnes, A.; Provost, E.; Fürst, W.; Cote, G. Modelling of uranium(VI) extraction by D2EHPA/TOPO from phosphoric acid within a wide range of concentrations. *Hydrometallurgy* **2016**, *165*, 57–63.
- (18) Meridiano, Y.; Berthon, L.; Crozes, X.; Sorel, C.; Dannus, P.; Antonio, M. R.; Chiarizia, R.; Zemb, T. Aggregation in organic solutions of malonamides: Consequences for water extraction. *Solvent Extr. Ion Exch.* **2009**, *27*, 607–637.
- (19) Quinn, J. E.; Soldenhoff, K. H.; Stevens, G. W.; Lengkeek, N. A. Solvent extraction of rare earth elements using phosphonic/phosphinic acid mixtures. *Hydrometallurgy* **2015**, *157*, 298–305.
- (20) Prochaska, K. Interfacial activity of metal ion extractant. *Adv. Colloid Interface Sci.* **2002**, *95*, 51–72.
- (21) Su, W.; Chen, J.; Jing, Y. Aqueous Partition Mechanism of Organophosphorus Extractants in Rare Earths Extraction. *Ind. Eng. Chem. Res.* **2016**, *55*, 8424–8431.
- (22) Hyde, S. T.; Barnes, I. S.; Ninham, B. W. Curvature Energy of Surfactant Interfaces Confined to the Plaquettes of a Cubic Lattice. *Langmuir* **1990**, *6*, 1055–1062.
- (23) Krimm, S. *The hydrophobic effect: Formation of micelles and biological membranes*; Charles Tanford, Wiley-Interscience: New York, 1980.
- (24) Zemb, T. N. The DOC model of microemulsions: Microstructure, scattering, conductivity and phase limits imposed by steric constraints. *Colloids Surf., A* **1997**, *129–130*, 435–454.
- (25) Bley, M.; Siboulet, B.; Karmakar, A.; Zemb, T.; Duffrêche, J.-F. A predictive model of reverse micelles solubilizing water for solvent extraction. *J. Colloid Interface Sci.* **2016**, *479*, 106–114.
- (26) Karmakar, A.; Duvail, M.; Bley, M.; Zemb, T.; Duffrêche, J.-F. Combined supramolecular and mesoscale modelling of liquid-liquid extraction of rare earth salts. Manuscript in preparation.
- (27) Duvail, M.; van Damme, S.; Guilbaud, P.; Chen, Y.; Zemb, T.; Duffrêche, J.-F. The role of curvature effects in liquid-liquid extraction: assessing organic phase mesoscopic properties from MD simulations. *Soft Matter* **2017**, *13*, 5518–5526.
- (28) Marcus, Y. *Ions in Solution and their Solvation*; John Wiley & Sons Inc.: New York, 2015.
- (29) Hansen, J.-P.; McDonald, I. R. *Theory of Simple Liquids*, 3rd ed.; Academic Press: Burlington, 2006.
- (30) Vafaei, S.; Tomberli, B.; Gray, C. G. McMillan-Mayer theory of solutions revisited: Simplifications and extensions. *J. Chem. Phys.* **2014**, *141*, 154501.
- (31) Leodidis, E. B.; Hatton, T. A. Amino acids in AOT reversed micelles. 1. Determination of interfacial partition coefficients using the phase-transfer method. *J. Phys. Chem.* **1990**, *94*, 6400–6411.
- (32) Moeser, B.; Horinek, D. Biophysical Chemistry The role of the concentration scale in the definition of transfer free energies. *Biophys. Chem.* **2015**, *196*, 68–76.
- (33) Ellis, R. J.; Meridiano, Y.; Muller, J.; Berthon, L.; Guilbaud, P.; Zorz, N.; Antonio, M. R.; Demars, T.; Zemb, T. Complexation-induced supramolecular assembly drives metal-ion extraction. *Chem. - Eur. J.* **2014**, *20*, 12796–12807.
- (34) Li, J.; Wang, X.; Zhao, G.; Chen, C.; Chai, Z.; Alsaedi, A.; Hayat, T.; Wang, X. Metal-organic framework-based materials: superior adsorbents for the capture of toxic and radioactive metal ions. *Chem. Soc. Rev.* **2018**, *47*, 2322–2356.
- (35) Ellis, R. J.; Meridiano, Y.; Chiarizia, R.; Berthon, L.; Muller, J.; Coustou, L.; Antonio, M. R. Periodic behavior of lanthanide coordination within reverse micelles. *Chem. - Eur. J.* **2013**, *19*, 2663–2675.
- (36) Dill, K. A.; Bromberg, S. *Molecular Driving Forces: Statistical Thermodynamics in Biology, Chemistry, Physics, and Nanoscience*, 2nd ed.; Garland Science: Boca Raton, FL, 2011.
- (37) Chen, Y.; Duvail, M.; Guilbaud, P.; Duffrêche, J.-F. Stability of reverse micelles in rare-earth separation: a chemical model based on a molecular approach. *Phys. Chem. Chem. Phys.* **2017**, *19*, 7094–7100.
- (38) Lipfert, J.; Columbus, L.; Chu, V. B.; Lesley, S. A.; Doniach, S. Size and shape of detergent micelles determined by small-angle X-ray scattering. *J. Phys. Chem. B* **2007**, *111*, 12427–12438.
- (39) Berthon, L.; Martinet, L.; Testard, F.; Madic, C.; Zemb, T. Solvent penetration and steric stabilization of reverse aggregates based on the DIAMEX process extracting molecules: Consequences

for the third phase formation. *Solvent Extr. Ion Exch.* **2007**, *25*, 545–576.

(40) Ricoul, F.; Dubois, M.; Belloni, L.; Zemb, T.; Andre-Barres, C.; Rico-Lattes, I. Phase Equilibria and Equation of State of a Mixed Cationic Surfactant-Glycolipid Lamellar System. *Langmuir* **1998**, *14*, 2645–2655.

(41) Antonio, M. R.; Chiarizia, R.; Gannaz, B.; Berthon, L.; Zorz, N.; Hill, C.; Cote, G. Aggregation in solvent extraction systems containing a malonamide, a dialkylphosphoric acid and their mixtures. *Sep. Sci. Technol.* **2008**, *43*, 2572–2605.

(42) Meridiano, J. Organisation des molécules extractantes de type diamide: lien avec les propriétés extractantes?, Rapport CEA-R-6228. Ph.D. Thesis, Université Paris XI, 2009.

(43) Testard, F.; Bauduin, P.; Martinet, L.; Abécassis, B.; Berthon, L.; Madic, C.; Zemb, T. Self-assembling properties of malonamide extractants used in separation processes. *Radiochim. Acta* **2008**, *96*, 265–272.

(44) Ennis, J. Spontaneous Curvature of Surfactant Films. *J. Chem. Phys.* **1992**, *97*, 663–678.

(45) Zemb, T.; Duvail, M.; Dufrière, J.-F. Reverse Aggregates as Adaptive Self-Assembled Systems for Selective Liquid-Liquid Cation Extraction. *Isr. J. Chem.* **2013**, *53*, 108–112.

(46) Nagarajan, R. Molecular packing parameter and surfactant self-assembly: The neglected role of the surfactant tail. *Langmuir* **2002**, *18*, 31–38.

(47) Muller, J. M.; Berthon, C.; Couston, L.; Zorz, N.; Simonin, J. P.; Berthon, L. Extraction of Lanthanides(III) by a Mixture of a Malonamide and a Dialkyl Phosphoric Acid. *Solvent Extr. Ion Exch.* **2016**, *34*, 141–160.

(48) Déjugnat, C.; Dourdain, S.; Dubois, V.; Berthon, L.; Pellet-Rostaing, S.; Dufrière, J.-F.; Zemb, T. Reverse aggregate nucleation induced by acids in liquid-liquid extraction processes. *Phys. Chem. Chem. Phys.* **2014**, *16*, 7339.

(49) Tanford, C. *The Hydrophobic Effect: Formation of Micelles and Biological Membranes*, 2nd ed.; Garland Science: Boca Raton, FL, 1980.

(50) Rey, J.; Dourdain, S.; Berthon, L.; Jestin, J.; Pellet-Rostaing, S.; Zemb, T. Synergy in Extraction System Chemistry: Combining Configurational Entropy, Film Bending, and Perturbation of Complexation. *Langmuir* **2015**, *31*, 7006–7015.

(51) Dourdain, S.; Déjugnat, C.; Berthon, L.; Dubois, V.; Pellet-Rostaing, S.; Dufrière, J.-F.; Zemb, T. Liquid-Liquid Extraction of Acids by a Malonamide: II-Anion Specific Effects in the Aggregate-Enhanced Extraction Isotherms. *Solvent Extr. Ion Exch.* **2014**, *32*, 620–636.

(52) Bosland, L. Etude thermodynamique et cinétique de l'extraction des nitrates de lanthanides par un malonamide (N, N diméthyl-N, N dioctylhexylethoxy malonamide ou DMDOHEMA), Rapport CEA-R-6099. Ph.D. Thesis, Ecole Centrale Paris, 2006.

(53) Cuillerdier, C.; Musikas, C.; Hoel, P.; Nigond, L.; Vitart, X. Malonamides as New Extractants for Nuclear Waste Solutions. *Sep. Sci. Technol.* **1991**, *26*, 1229–1244.

(54) Rydberg, J.; Cox, M.; Musikas, C.; Choppin, G. R. *Solvent Extraction Principles and Practice, Revised and Expanded*; Taylor & Francis: Boca Raton, FL, 2004; DOI: 10.1201/9780203021460.

(55) Condamines, N.; Musikas, C. *Solvent Extr. Ion Exch.* **1992**, *10*, 69–100.

(56) Tian, Q.; Hughes, M. A. The mechanism of extraction of HNO<sub>3</sub> and neodymium with diamides. *Hydrometallurgy* **1994**, *36*, 315–330.

(57) Panak, P. J.; Geist, A. Complexation and extraction of trivalent actinides and lanthanides by triazinylpyridine N-donor ligands. *Chem. Rev.* **2013**, *113*, 1199–1236.

(58) Kaufholz, P.; et al. Solvent Extraction and Fluorescence Spectroscopic Investigation of the Selective Am(III) Complexation with TS-BTPhen. *Solvent Extr. Ion Exch.* **2016**, *34*, 126–140.

(59) Lu, Y.; Liao, W. Extraction and separation of trivalent rare earth metal ions from nitrate medium by p-phosphonic acid calix[4]arene. *Hydrometallurgy* **2016**, *165*, 300–305.

(60) Spadina, M.; et al. Rare earth elements predictive extraction: the case of charged extractants. Manuscript in preparation.

(61) Press, W. H.; Teukolsky, S. A.; Vetterling, W. T.; Flannery, B. P. *Numerical Recipes in Fortran77: The Art of Scientific Computing*, 2nd ed.; Cambridge University Press: New York, 1992.